PPPL-3278, Preprint: January 1998, UC-426

The TFTR E||B Spectrometer for Mass and Energy Resolved Multi-Ion Charge Exchange Diagnostics

S.S. Medley and A.L. Roquemore

Princeton Plasma Physics Laboratory, P. O. Box 451, Princeton, NJ 08543 USA

Abstract

The Charge Exchange Neutral Analyzer diagnostic for Tokamak Fusion Test Reactor was designed to measure the energy distributions of both the thermal ions and the supra thermal populations arising from neutral beam injection and ion cyclotron radio frequency heating. These measurements yield the plasma ion temperature as well as several other plasma parameters necessary to provide an understanding of the plasma condition and the performance of the auxiliary heating methods. For this application, a novel charge exchange spectrometer using a dee-shaped region of parallel electric and magnetic fields was developed at the Princeton Plasma Physics Laboratory. The E||B spectrometer has an energy range of $0.5 \leq A(\text{amu})E(\text{keV}) \leq 600$, and is designed to provide mass-resolved energy spectra of H^+, D^+, and T^+(or $^3He^+$) ion species simultaneously during a single discharge. The detector plane exhibits parallel columns of analyzed ions, each column containing the energy dispersed ions of a given mass-to-charge ratio. The detector consists of a large area microchannel plate which is provided with three rectangular, semi-continuous active area strips, one coinciding with each of the mass columns for detection of H^+, D^+, and T^+ and each mass column has 75 energy channels. The design and performance of the E||B spectrometer is described in detail, including the effects of exposure of the microchannel plate detector to magnetic fields, neutrons and tritium.

I. INTRODUCTION

In contemporary tokamaks and other magnetic confinement devices, the extensive use of neutral beam injection and radio frequency auxiliary heating generates multispecies plasmas containing both thermal and non thermal ion energy distributions. This has driven significant changes in the requirements for many magnetically confined fusion plasma diagnostics[1]. In the area of charge exchange diagnostics, this imposed a need to extend the capabilities of spectrometers used for neutral particle analysis. Prior to this time, the spectrometer requirements were adequately satisfied either by magnetic momentum analyzers[2] or by electrostatic energy analyzers with a variety of geometries including cylindrical plate[3-5], parallel plate[6], and retarding-field gridded systems[7]. With beam heating, the need for mass resolution became prevalent, due to the fact two-ion component plasmas became commonplace wherein the energy distributions of the beam slowing-down particles and the Maxwellian plasma bulk ions strongly overlapped. Frequently the hydrogenic ion species for the beam and target plasma were different. In cases where they were the same (e.g. D-D), the residual population of other ions (e.g. H) could often be exploited for ion temperature measurements. To provide both mass and energy analysis capability for charge exchange spectrometers, the initial approach was to precede the electrostatic system (typically cylindrical condenser) with a magnetic field[8]. In such configurations, the magnetic and electric fields were orthogonal to each other and the resulting instrument had several disadvantages: a) the cylindrical condensers were complicated to fabricate and align, b) the spatially separated magnetic and electrostatic field regions led to relatively large spectrometer dimensions, and c) only a single ion species could be detected at a time.

The requirements for the charge exchange system for the Tokamak Fusion Test Reactor (TFTR) were considerably more involved than for preceding devices due to the provision for operation using combinations hydrogen, deuterium, or tritium for either the neutral beam injectors or the target plasma. Also, production of energetic ions tails using ICRF heating of H, ^{3}He, and T minorities needed to be accommodated. For TFTR, a novel Charge Exchange Neutral Analyzer (CENA) concept, using a dee-shaped region of parallel electric and magnetic fields (E||B), was developed at the Princeton Plasma Physics Laboratory (PPPL)[9,10]. The E||B analyzer has an energy range of $0.5 \leq A(amu)E(keV) \leq 600$, and its design enables simultaneous mass-resolved measurements of H. D, and T (or 3He) energy spectra during a single discharge. A further innovation was utilization of large-area, high-gain, multi-channel, single-particle detector arrays[11] using microchannel plate technology[12]. Prior to the start of TFTR operation, an E||B prototype[13] was operated on the Princeton Large Torus (PLT). In addition, a variation of the E||B concept in which the parallel magnetic and electric fields were spatially separated was implemented on the charge exchange analyzers for the Poloidal Divertor Experiment (PDX) device, replacing an earlier design using cylindrical electrostatic plates[14].

Since the development of the E||B design concepts at PPPL, charge exchange spectrometers using parallel magnetic and electric fields, either spatially superimposed or sequential, have gained widespread acceptance in the magnetic confinement fusion research community. Replicas of the TFTR-style (superimposed field regions) E||B spectrometers constructed by PPPL have been implemented on ORNL-Stellarator[15, 16] and Alcator C-Mod[17] and adaptations of this design have been implemented on JT-60[18] and TMX-U[19]. The PDX-style (sequential field regions) E||B spectrometers built at PPPL have been installed on Alcator C-Mod[15] and Tokamak de Varennes[20, 21]. Similar instruments utilizing this concept have been developed for JET[22], JFT-2[23] and for high energy alpha particle diagnostics at the A. F. Ioffe Physical-Technical Institute[24].

A different approach to devising advanced neutral particle diagnostics used an electrostatic time-of-flight analyzer spectrometer[25,26]. In this approach, energy analysis is provided by curved electrostatic plates and utilization of the coincidence technique to measure the time-of-flight of the reionized neutral during their transit within the spectrometer provides mass resolution. A particular advantage of this approach is the capability to discriminate the particle signal from random signals due to large neutron and gamma radiation backgrounds typical of fusion experiments.

The purpose of this paper is to present a comprehensive description of the design and calibration of the E||B spectrometer and to illustrate application of the instrument on TFTR. The principle of operation of the spectrometer is presented in Sec. I followed by a description of the design of the spectrometer (Sec. II), the microchannel plate detector (Sec. IV), and the instrumentation and control system (Sec. V). Calibration of the instrument including the effect of spectrometer magnetic fringe fields on the performance microchannel pate detector is described in Sec. VI. The effects of exposure of the microchannel plate detector to neutron and gamma radiation and to tritium is discussed in Sec. VI. Finally, examples illustrating the range of applications of the E||B spectrometer to measurement of thermal and non thermal ion energy distributions on TFTR are given in Sec. VIII.

II. PRINCIPLE OF OPERATION OF THE E||B MASS AND ENERGY ANALYZER

The basic operating principle of the dee-shaped, superimposed parallel electric and magnetic field analyzer configuration is illustrated in Fig. 1. After reionization of the charge exchange neutrals in the stripping cell, the ions enter perpendicularly into a semi-circular region of parallel magnetic and electric fields. In these fields, the Lorentz forces

$$m d\underline{v}/dt = q(\underline{v} \times \underline{B} + \underline{\mathcal{E}}) \tag{1}$$

are not coupled. While traversing an arc of 180^o due to the magnetic field $\underline{B}$, the ions are displaced parallel to the electric field $\underline{\mathcal{E}}$. The time-of-flight

$$t_j = (\pi/B)\left[m/e\right]_j \tag{2}$$

between entering and exiting the field region is independent of the initial velocity for any given ion species $(m/e)_j$. The displacement Y_j of the j-th species parallel to the electric field is given by

$$Y_j = (\pi^2/2)\left[\mathcal{E}/B^2\right]\left[m/e\right]_j \tag{3}$$

which is also independent of velocity, so that all particles of a given m/e ratio are displaced along the electric field direction by the same amount. The ion species $(m/e)_j$ entering with velocity v_k is displaced along the detector plane a distance

$$Z_{jk} = (2/B)\left[m/e\right]_j v_k \tag{4}$$

from the entrance point in a direction perpendicular to $\underline{v}_k \times \underline{B}$. The collection plane thus exhibits parallel columns of analyzed ions, each column containing the energy dispersed ion of a given (m/e) ratio. The detector is located in the collection plane and consists of a planar Channel Electron Multiplier Array (CEMA) which is provided with three rectangular, semi-continuous active area strips, one coinciding with each of the mass columns for detection of H^+, D^+, and T^+. Each strip is divided into multiple elements of width ΔZ_j. The energy resolution

$$\Delta\mathcal{E}/\mathcal{E} = \pm\, \Delta Z_j/Z_j \tag{5}$$

where $\mathcal{E} = m(v_k)^2/2$ is therefore a function of displacement along each mass column.

Adequate spatial separations of the H^+, D^+, and T^+ ion species for the TFTR E||B design results in a relatively large magnet gap. From the relation for the magnetic field strength B (Gauss),

$$B = 1.25\ (NI/d) \tag{6}$$

it is evident that to provide a specified field using a set number of coil turns, N, the required energizing current I(A) is proportional to the pole separation d(cm). In addition to the sizable magnet power requirements arising from a large pole gap, the associated fringe field might be expected to adversely affect the ion trajectories. Alternative configurations are possible which reduce the pole separation while preserving the E||B analyzer concept[27, 28]. First, some degree of reduction in pole separation can be achieved by requiring that only part of the necessary spatial dispersion of the ion species takes place while the ions are traveling between the poles. The remainder of the dispersion is realized by allowing the ions to drift some distance on exiting the field region before striking the detector. If the detector plane remains parallel to, but is displaced away from the straight edge of the magnet. the mass columns become parabolic in shape, with lower energies having a greater displacement in the direction of the electric field. Linear mass columns may be recovered, however, by tilting the detector plane about an axis which is parallel to the field direction and passes through the "entry point" of the ions into the magnet gap[29]. The greatest reduction in pole separation is achieved by applying the electric field after the ions emerge from the magnetic field[13, 22-24]. With both alternatives, the price for relaxing the magnetic fringe field effects is a significant increase in the overall dimensions of both the analyzer and the detector to encompass the same energy range. Since the application to tokamaks requires shielding the interior of the analyzer against stray magnetic fields, increasing the size of the analyzer also leads to more massive shielding enclosure walls.

III. TFTR E||B SPECTROMETER DESIGN

The Charge Exchange Neutral Analyzer for TFTR was designed to measure H^+, D^+, and T^+(or $^3He^+$) ion species simultaneously with up to 75 energy channels per ion and an energy range of $0.5 \leq A(amu)E(keV) \leq 600$. The schematic in Fig. 2 shows plan and elevation cross sections of the E||B analyzer with the insert (not to scale) showing the geometry of the microchannel plate detector. The smaller chamber houses a 25 cm long stripping cell typically operated at 1-3 mTorr helium. This arrangement facilitate differential pumping to reduce streaming of the stripping cell gas into the main chamber of the spectrometer or into the TFTR vacuum vessel. The main chamber which contains the field region and the detector is approximately 90 cm long by 60 cm wide by 23 cm deep.

The 60 cm diameter dee-shaped electromagnet is energized by two 72-turn coils, one mounted on each of the magnet pole pieces. A stainless steel shroud welded to the pole piece on one edge and to the spectrometer wall on the other isolates the coil from the vacuum region. The 3.2 cm thick soft iron walls of the spectrometer provide the return yoke for the electromagnet. A 72-turn coil consists of two 36-turn coils electrically connected in series, but with each 36-turn coil having a separate water cooling path. Coil windings are fabricated using 0.48 cm square copper with a 0.24 cm diameter cooling channel. The water cooled coil windings require an inlet pressure of 220 psi at 50 ^{o}F with a flow rate of 0.6 gpm yielding an outlet temperature of 160 ^{o}F during steady state operation at full field.

The electric field is produced between one magnet pole face at ground potential and a negatively biased, dee-shaped electrode mounted against, but electrically insulated from, the opposite pole face. The ion beam enters near the ground electrode for two reasons. First, this location reduces perturbation of the incoming particle energy due to the electrode potential. Second, this arrangement permits utilization of the full separation of the magnet gap.

The basic performance requirements of the vacuum system[30] for the spectrometers is as follows. Under a gas load (typically helium) of 1-5 mTorrl/s due to the stripping cell, the analyzer enclosure and the flight tube connecting the spectrometer to the torus should be maintained at $\leq 10^{-6}$ Torr. The quantity of gas from the analyzers which can be permitted to enter the torus must be minimized. A design goal of 10^{-4} Torrl/s was adopted, which corresponds to a torus partial pressure of ~ 10^{-9} Torr due to the working gas load from the charge exchange diagnostic. The vacuum system was designed so that during tritium operation in TFTR, the partial pressure of tritium introduced into the analyzers would be below 10^{-8} Torr in order for the background count rate of the detector induced by beta decay of tritium to be negligible.

A photograph of the E||B spectrometer is shown in Fig. 3 and a list of the salient parameters of the spectrometer is given in Table I.

IV. MICROCHANNEL PLATE DETECTOR DESIGN

In recent years, the application of microchannel plate (MCP) electron multipliers to the detection of particles and photons has expanded in many areas of science and technology[12]. One of the advantages of MCP detectors compared with conventional electron multiplier tubes is a relatively high insensitivity to operation in a magnetic field environment. Sufficiently strong magnetic fields ($\geq$ 100 Gauss) such as encountered for diagnostics in the vicinity of magnetic confinement fusion experiments, however, can degrade the performance characteristics of MCP detectors. In general, the MCP gain decreases in strong magnetic fields and the drop is more rapid for fields parallel to the microchannel pores compared with transverse fields.

For detection of the mass and energy analyzed ions, the E||B analyzer employs large area microchannel plates fabricated by Galileo Electro-Optics Corp., Sturbridge, MA 01518. An isometric blowup of the chevron MCP assembly is shown in Fig. 4 and a list of the salient parameters is given in Table II. The 4.6 x 13 cm front (B) and rear(D) plates were sliced on an 8^{o} bias with respect to the bore of the 25 m diameter microchannels. Operating voltages are applied at the front (A), intermediate (C), and rear (E) electrodes. The front electrode also serves as part of the assembly hardware while the intermediate electrode provides a mask defining the desired active area of the MCP. The multianode collector is comprised of 75 independent anodes of area 0.4 cm^2 each (0.4 x 1.0 cm) which are arrayed in three columns of 25 anodes per column. The center-to-center- separation is 1.5 cm for the columns and 0.5 cm for the anodes within a column. The separation between adjacent anodes is 0.1 cm. A guard electrode surrounding each anode and extending over the inactive MCP region is provided to suppress interanode cross talk. The anode pads and guard electrode (F) are formed by evaporating gold onto a ceramic substrate (G) fitted with signal connector pins extending to the backside of the substrate. Three such arrays are mounted in tandem to form the complete E||B detector array with a total length of 39 cm as shown in the photograph in Fig. 5. Each subsection is independently biased. With the chevron microchannel plate configuration, detection of ion flux levels of 10^3 - 10^6 ions/cm^2/s are anticipated with detection efficiency approaching 100%.

The MCP has a modal gain of ~ 5 x 10^6 electrons/ pulse, and is operated in the pulse counting (single particle detection) mode at rates up to 10^6 count/cm^2/s. The signal processing electronics for each anode consists of a charge-sensitive buffer circuit located inside the vacuum at the backside of the detector and a pulse preamplifier/discriminator (PAD) module located in a bin close to the analyzer. The buffer converts charge pulses to voltage pulses and minimizes pulse distortion by matching its output impedance to that of the cable attaching the buffer to the PAD. The PAD circuit, based on the LeCroy MVL 100 (100x gain, 1- MHz bandpass) converts the voltage pulse to a differential TTL pulse having a fixed width of 125 ns for transmission over long data lines (~ 30 m) to a scalar/memory modules outside the TFTR machine area.

V. INSTRUMENTATION AND CONTROL

A block diagram of the overall instrumentation and control system for an E||B spectrometer in the TFTR charge exchange analyzer system is shown in Fig. 6. This instrumentation was remotely controlled[31] through CICADA, the TFTR Central Instrumentation and Control and Data system. The devices have been grouped according to the labels on the right of the figure. Multiple analyzers interface to the TFTR torus through a plenum having a dedicated vacuum system shown at the bottom of the figure. Each analyzer has a dedicated vacuum system, with separate ionization gauges to measure the pressure in the stripping cell and in the main spectrometer chamber. A plenum valve control provided connection between the individual analyzer and plenum vacuums with interlock logic to ensure compatible vacuum conditions to open the plenum valves. The magnetic field system includes a 250A/80V DC power supply, and a Hall probe mounted on one of the pole pieces to measure the magnetic field strength. A flow meter and a thermocouple in the magnet water cooling system provide interlocks to the magnet power supply to guard against coolant loss or magnet over heating. The high voltage power supplies for the electric field and for biasing the microchannel plates are commercial CAMAC components. The 12-bit, 8 MHz scalar memory modules for data acquisition were custom built to TFTR specifications. The MCP voltage divider splits the output from a LeCroy HV module into the three bias voltages applied to the MCP plates. The MCP crowbar is designed to remove the high voltage bias from the MCP voltage divider and to provide a fast discharge path for the charged cable capacitance. Crowbar control is achieved through interlock with a vacuum trip relay on the ion gauge controller monitoring the vacuum in the main spectrometer chamber. The crowbar will disconnect the power supply and discharge 10,000 pF of load capacitance in less than 5 ms.

VI. CALIBRATION

Although this section presents the calibration results for the TFTR E||B spectrometer, it is opportune to first describe certain effects on the calibration process arising from the spectrometer magnetic fringe field in the vicinity of the microchannel plate detector.

During calibration of the E||B analyzer, a new effect of magnetic fields on the operation of MCP detectors was discovered. Using a multianode MCP operated in a transverse magnetic field, we observed that excitation of one area of the MCP by a collimated ion beam produced ghost images of the beam at locations on the MCP several centimeters removed from the ~ 4 mm diameter beam impact region[32]. The ghosts images are created by secondary electrons which are produced at the surface of the MCP and returned to another location on the plate surface under the influence of the EXB fields, where E is the electric field perpendicular to the plate due to the MCP bias potential of and B is the ambient transverse magnetic fringe field of the analyzer.

In other words, a regenerative process is observed in which the secondary electrons produced at the interstitial spaces of the MCP traverse the surface of the plate in the EXB direction by multiple 'gyro orbit' steps.

The applied -2100 volt MCP bias and the transverse component (~ 50 - 100 Gauss) of the spectrometer magnetic fringe field create an EXB field region that causes the particles to execute semicircular gyro orbits and return to the plate an orbit diameter away from the production point. On returning to the MCP surface, a portion of the secondary electrons will enter the pores of the plate a generate an output pulse, while the remainder will impact on the interstitial spaces creating a new generation of secondary electrons with trajectories similar to the first generation. This process was observed to repeat itself up to seven times before the gyro peak amplitude approaches zero. In addition, 'spillover' gyro orbit signals were observed on the anode strings in the secondary 'mass columns' adjoining the column receiving the ion beam, although with significantly reduce amplitude relative to those observed within the primary mass column. Increasing the analyzer magnetic field caused the spacing between the gyro peaks to be compressed, as expected. To suppress the gyro-electron effect, a double-walled soft iron shield was placed around the MCP with a window cut out to admit the particles. This window was covered by a grounded, high transparency mesh. The residual magnetic field inside the shield was measured to be ~ 10 Gauss for the maximum spectrometer operation field of 5 kG.

An alternate method to eliminate the gyro peaks without requiring magnetic shielding of the MCP was investigated which involved reversing the bias on the MCP by placing a +2100 volt bias on the output anode surface and grounding the input surface. In this scheme, the individual signal anodes need to be capacitively coupled to the signal processing electronics to block the applied bias. The gyro peak effect was eliminated by this approach, but care must be taken to avoid anode cross talk due to capacitive coupling.

In addition to the effect of the exit magnetic fringe field on the MCP detector, perturbation of the ion trajectory in the spectrometer arises due to both the entrance and exit fringe field regions. Trajectory perturbations at the entrance to the dee-shaped field region are particularly troublesome because of the relatively long flight path lengths (~ 30 - 160 cm) inside the magnet poles, which causes small perturbations at the entrance to produce significant deviations in the detector plane. This problem was effectively eliminated by introducing a "snubber" at the magnet entrance which consisted of a 3 cm wide by 6 cm high by 15 cm long block of annealed soft iron with a 3 mm diameter channel bored through to long dimension to allow passage of the ion beam. The exit field problem is less critical and trajectory perturbations were effectively suppressed as a byproduct of the magnetic shielding installed around the MCP to solve the gyro effect discussed above. However, a residual fringe field perturbation exists for small radius ion trajectories which results in the "flyback effect" discussed below.

For initial calibration, tracking of ions in the detector plane was examined visually by substituting a phosphor screen for the CEMA detector. The screen consisted of a thin film of Willemite deposited on 6 cm x 13 cm x 0.3 cm quartz plate and overlayed with a conductive coating of aluminum. The aluminized surface was biased to -2100 volts during testing to simulate the bias voltage that will exist of the front surface of the CEMA detector. Microampere beam spots of ~ 3 mm diameter were visible over an energy range of 10 - 150 keV with this arrangement.

The analyzer was calibrated from 0.5 to 150 keV for both hydrogen and deuterium to determine the energy, energy resolution, and total detection efficiency for a range of analyzer magnetic and electric field setting (Figs. 7 - 10). The energy as a function of anode position was in agreement with Eq. 7 except for minor deviations at small Larmor radii. The measured energy dynamic range was $E_{max/Emin}$ = 30, where E_{max} and E_{min} are the maximum and minimum energies that can be measured simultaneously. The FWHM energy resolution $\Delta E/E$ varied from 16 to 4 % from the low to the high energy end of the detector. The observed mass rejection was 1000:1.

The total relative efficiency (detector counts/neutral), measured over an energy range of 0.5 - 150 keV at a helium stripping cell pressure of 3 mTorr, is shown Fig. 10. The data shown represents an average of the results obtained for calibration of four E||B spectrometers of identical construction. Error bars indicate the scatter in the calibration data of these four systems. The analyzer efficiency has been sucessfully modeled over the entire range of energy by using published cross sections and assuming helium pressure of ~ 3 mTorr for the 25 cm long cell, provided measured scattering cross sections are included[15].

VII. RADIATION EFFECTS

As part of the development of the E||B spectrometer for application on TFTR, particularly during deuterium-tritium operation, studies were made of the reponse of the microchannel plate detector under exposure to 2.5 and 14 MeV neutron irradiation and to tritium gas. Although unwanted response effects were observed in both cases, they did not preclude extensive application of the microchannel plates in the E||B spectrometer on TFTR.

VIIa. Neutron Response

High levels of neutron and neutron-induced gamma-ray fluxes during both DD and particularly DT operation of TFTR have been a source of high-level noise counts for many diagnostics. Typical source strengths are ~ 2×10^{16} n/s for 2.45 MeV neutrons during DD operation and ~ 2×10^{18} n/s during DT operations with roughly equivalent gamma-ray yields in the respective cases. During TFTR experiments involving D-T discharges, the 14 MeV neutron flux levels in the environment of the CEMA detector reach ~10^{11} neutrons/cm^2/s. The TFTR charge exchange neutral analyzer (CENA) utilizes a large-area microchannel plate detector which responds to energetic neutron and gamma rays. An investigation of the neutron response of the CEMA showed measured neutron detection efficiencies of 1.7 x 10^{-3} and 6.4 10^{-3} counts/neutron for 2.5 MeV-DD and 14 MeV-DT neutrons, respectively[11].

We adopted the convention that reliable results can no longer be obtained when total signal levels caused the MCP to deviate from linear response by more than 20%. This typically occurs for total neutron production rates of ~ 4×10^{15} n/s in DD discharges. By extrapolating to DD Q~1 equivalent discharges with an anticipated neutron production rate of ~ 10^{17} n/s, it was established that for reliable MCP operation a radiation shield enclosure (Fig. 11) capable of attenuating the noise level by approximately two orders of magnitude would be required. A shield to suppress neutron and gamma induced noise in the MCP was designed and implemented which consisted of 10-cm-thick inner housing of lead surrounded by a 23-cm-thick layer of 1.0% borated polyethylene. This shielding provided a measured reduction of 140x in the MCP noise level relative to an unshielded analyzer[33]. Even greater shielding would have been required if the system had been operated in DT discharges.

A correction for the residual neutron and gamma induced noise signal is facilitated by using 'masked' detectors which respond only to the neutron and gamma radiation so that the noise levels monitored as a function of time during the discharge. Using the relative neutron/gamma sensitivity of the individual charge exchange signal channel to the masked detectors determined by calibration shots, a time dependent correction for noise on the raw charge exchange signal is obtained.

VIIb. Tritium Effects

The TFTR E||B spectrometers were designed at the outset to be compatible with tritium operation in TFTR, although the system was prematurely decommissioned due to the cost of implementing the neutron and gamma shielding that was essential for D-T operation. In preparation, however, an investigation was sponsored to study the effects of low pressure tritium exposure on the operation of the MCP detectors used in the E||B spectrometers[34]. The beta decay of tritium could result in undesired background count rates which could potentially obscure detection of low level signals. Computer simulations[29] of the charge exchange system predicted a tritium pressure pulse of ~2 x 10^{-8} Torr inside the spectrometer during a D-T discharge on TFTR. In the study, a chevron MCP was exposed to tritium at pressures between 5.5 x 10^{-9} Torr and 9 x 10^{-7} Torr, resulting in cumulative exposures up to ~ 0.1 Torr-s. Two types of responses were observed; namely, 1) a reversible counting rate which was proportional to the tritium pressure as shown in Fig. 12 and disappeared when the tritium was removed, and 2) an essentially irreversible rate which gradually increased with cumulative exposure as shown in Fig. 13 and which persisted even when the tritium was removed. Pulse height spectra taken during the exposures indicated that the irreversible response was due to changes within the MCP and not related to tritium adsorbed on surfaces of nearby structures. An extended bakeout sequence for 4 days at 140 C reduced the background count rate by a factor of ~4, Even at this level, however, the background count rate was ~ 300 cps compared with the normal 'background' count rate of ~ 1 cps for an unexposed MCP. This irreversible behavior can certainly be expected to limit the useful life time of MCP's which are exposed to tritium in fusion experiments. Some highlights of the study were:

- The pulse height spectrum exhibits a "Gaussian" shape for the reversible tritium-induced background and an "exponential" shape for the irreversible exposure effect.

- The reversible background appears to be caused by collected slow ions, rather than fast electrons due to beta decay.

- The irreversible background count rate is attributed to tritium decay in OT hydroxyls formed by tritium exchange with hydrogen hydroxyls present in MCP glasses.

- The tritium-induced count rate is affected by 'environmental' factors such as the chamber volume, wall proximity, and ambient electromagnetic fields.

- Extension of the bakeout time results in a decrease in the rate and amplitude of the irreversible background pulses.

VIII. APPLICATION ON TFTR

The charge exchange neutral analyzer (CENA) diagnostic for TFTR provides two autonomous analyzer systems and one shared diagnostic neutral beam (DNB). The first system emphasizes the measurement of ion phenomena associated with neutral beam injection and has a fanlike field of view along six sightlines in the equatorial plane which are capable of being scanned in both the toroidal and vertical directions (Fig. 14). The second system measures the perpendicular ion energy distribution (e.g. plasma ion temperature and RF-driven energetic ion tails) along as many as 12 vertical line-of-sight chords spaced approximately equidistantly across the torus minor diameter (Fig. 15). Each of the charge exchange lines-of-sight can be provided with an identical but independent CENA spectrometer. The DNB provides a time-modulated, spatially localized enhancement of the charge exchange efflux and is steerable in order to access the viewing field of either CENA system[35]. The DNB operates at 80 keV beam energy with a 10 x 10 cm ion source extraction grid geometry to provide a total extracted ion current of ~ 15A for deuterium and ~ 17A for hydrogen.The data reduction methods for active and passive charge exchange measurements using the pulse counting mode of data acquisition has been described in detail elsewhere[14]. Values of the cross sections of the various charge changing reactions needed in this analysis are obtained from published data[36]. The E||B charge exchange diagnostic systems on TFTR have been used to investigate a broad range of ion-related phenomena, such as the ion temperature in ohmic and beam heated discharges[7, 37-38], adiabatic toroidal compression experiments[39], RF heating[40-42], and MHD effects such as fishbones[43]. Some typical data are shown for beam injection discharges (Fig. 16), and passive (Fig. 17) and active (Fig. 18) ion temperature measurements.

Adiabatic toroidal compression experiments were performed in conjunction with high power neutral beam injection in TFTR[39]. During magnetic compression (C = 1.38) of NBI plasmas, acceleration of 80 keV beam ions up to 150 keV is observed, consistent with the C^2 prediction for ion acceleration. Using assumptions of conservation of angular momentum and magnetic moment to vary the beam ion distribution in a bounce averaged Fokker-Planck program, the calculated fast ion slowing-down distributions agreed with the shape of the spectra from the charge exchange measurements.

Both the tangential and the vertical E||B charge exchange diagnostics were used to measure the radial diffusivity of fast ions during neutral beam injection on TFTR. TFTR edge heating experiments provided an opportunity for direct observation fast ion radial diffusion[44] using the tangential charge exchange system. For these experiments, a ring of fast ions (E = 95 keV) on the outer flux surfaces (r = 45 - 70 cm) into a plasma with R = 2.36 m, a = 0.7 m, I_p = 1.2 MA, B_T = 4.95 T, and $\langle n_e \rangle$ = 1.5 x

10^{19} m^{-3}. Horizontally-scanning charge exchange measurements of the neutral spectra near the inner major radius edge of the fast ion "fiery ring" (R_T = 1.9 m) showed a sharp decrease at the expected radius. Fast ion diffusion causes the measured edge of the fiery ring to become less steep at lower energies. This, a comparison of the neutral flux plotted against detector R_T at various energies provides a direct estimate of the diffusion when the measurements are compared with detailed Fokker-Planck simulation including a diffusion operator. Under the conditions of this experiment, the fast ion radial diffusion coefficient was determined to be < 0.1 m^2/s.

The temporal characteristics of the measured neutral particle flux have also been exploited for diffusion coefficient studies. Comparison of charge exchange measurements from both the horizontal[45] and vertical[46] systems with theoretical calculation showed that the spatially-averaged diffusion coefficient of fast ions is $\leq 0.10 \pm 0.05$ $m^2 s^{-1}$, which is approximately an order of magnitude less than the diffusion coefficient characteristic of thermal ions.

A modification of the E||B analyzer was used to characterize the ion species produced by the TFTR neutral heating beams[47, 48]. On a test stand for one of the TFTR beamlines, the target calorimeter had a 2.5-cm-diameter penetration on the beam axis to allow passage of beam particles into an E||B analyzer. The analyzer was a standard TFTR E||B type with a gas stripping cell, but the detectors were an array of Faraday cups that permitted the direct simultaneous measurement of the intense E, E/2, and E/3 components of the neutral beam. In addition, smaller Faraday cup arrays were configured for measuring the energy spread of the individual beam components. Species radial profile measurements could be performed by rastering the neutral beam across the collimator aperture.

During high power deuterium neutral beam heating of deuterium plasmas in TFTR, charge exchange measurement of the central ion temperature is difficult because the deuterium neutral energy spectrum is characteristic of the neutral beam slowing-down spectrum, and there is insufficient hydrogen flux [$H/(H + D) \leq 1.5\%$] to obtain a measurement from the background plasma. A solution was developed which involves fitting the deuterium slowing-down spectrum obtained from the horizontally viewing CENA's at energies above the neutral beam injection energy[49]. The slope of the ion energy spectra above the neutral beam injection energy is determined by a balance between the energy diffusion of the ions and the electron drag, resulting in an effective temperature which is a weighted average of the ion and electron temperatures. The ion temperature determined in this manner represents the central ion temperature if the neutral beam deposition is near the plasma center and if the measured charge exchange neutral flux arises from the plasma center. In TFTR, both of these requirements are satisfied. A brief description of this 'supra-NBI' technique is as follows. In the limit of pitch angle $v_{||}/v = \pm 1$:

$$f(E) \sim \exp(-\mathcal{E}/T_{eff}) \qquad (7)$$

where

$$T_{eff} = \frac{T_i + T_e(\mathcal{E}/\mathcal{E}_c)^{1.5}}{1 + (\mathcal{E}/\mathcal{E}_c)^{1.5} \pm \tau_s\, 9.58 \times 10^{11}\, [Z_b/A_b]\, [|E^*|/v_b]\, (\mathcal{E}/\mathcal{E}_c)^{1.5}.} \qquad (8)$$

In this equation T_i and T_e are the ion and electron temperatures, Z_b and A_b are the charge and mass of the neutral beam ions, $\mathcal{E}$ is the mean energy in the fit range used to evaluate T_{eff}, and $\mathcal{E}_c$ is the critical energy above which the effects of the electron drag on the beam ions are more important than the ion energy diffusion. $\mathcal{E}_c$ is defined as

$$\mathcal{E}_c = 14.8\, A_b \left([Z]/\langle A_i \rangle\right)^{2/3} T_e \qquad (9)$$

where A_b is the mass of the neutral beam ion and $[Z]/<A_i>$ is the average charge to mass ratio of the plasma given by

$$[Z]/<A_i> = \frac{\sum n_i (Z_i)^2 \ln \Lambda_i}{n_e A_i \ln \Lambda_e} \qquad (10)$$

The remaining term in the denominator accounts for the effects of the toroidal electric field, where τ_s is the slowing-down time of the fast ions, v_b is the beam ion velocity, and $|E^*| = |E|(1 - Z_b/Z_{eff})k$ where $|E|$ is the magnitude of the electric field in Volts/cm. The term containing the electric field is small ($O \sim 10^{-2}$ compared to unity) and was neglected in development of the supra-beam technique.

In the approximation where toroidal electric field and plasma rotation effects are negligible, The value of the ion temperature, T_i, is calculated from the slope of the distribution function above the neutral beam injection energy, T_{eff}, according to:

$$T_i \sim T_{eff} + (T_{eff} - T_e)\left[\mathcal{E}/\mathcal{E}_c\right]^{3/2}. \qquad (11)$$

The Fokker-Planck code modeling showed that the central ion temperature obtained from the high energy tangential deuterium charge exchange spectrum reproduces the central ion temperature remarkably well over a broad range of TFTR neutral beam and plasma discharge conditions. The code calculated T_i values fall within 10% of the input values for central plasma density variations from 0.5 - 1.5 x 10^{20} m^{-3}, density profiles of $(1 - r^2/a^2)^{\alpha}$ where α varies from 1 to 4, $2.5 < Z_{eff} < 4.5$, and plasma currents ranging from 0.85 - 2 MA. The calculated T_i values were insensitive to neutral beam power changes from 12 - 27 MW or to ± 10% changes of the neutral beam injection energy about a mean value. The study also showed that toroidal rotation affects the T_{eff} analysis and provides an analytical method to accomplish this correction. An example of the ion temperature measurements obtained with this technique is shown in Fig. 19.

ACKNOWLEDGMENTS

Work Supported by U.S. DoE Contract No. DE-AC02-76-CH0-3073. During the commissioning and operation of the E||B charge exchange diagnostic on TFTR from 1982-1992, numerous PPPL staff and collaborators from other organizations were involved. The authors gratefully acknowledge the contribution of R. Kaita, S.D. Scott, G.W. Hammett, W. Dorland, G. Schilling, C.L. Fiore (M.I.T.-P.F.C.), R.H. Radeztsky, M. Beer, C.E. Thomas (Georgia Institute of Technology), R. Persing, J. McEnerney, L. Lagin, J.A. Leine (Kalamazoo College), and G. Christianson.

TABLE I

E||B SPECTROMETER SPECIFICATIONS

<u>Mechanical</u>

Magnet pole radius:	30 cm(structural), 20 cm (working)
Magnet pole separation:	6 cm
Coil cross section:	4 cm x 6 cm
Turns per coil:	72 (2 coils)

<u>Electrical</u>

Maximum magnetic field:	5.5 kG
Ampere turns:	~ 14,00 per coil
Coil current:	0 - 200 A
Coil voltage:	40 - 60 V
Magnet power:	0 - 9 kW
Maximum electric field:	1 kV/cm
Maximum plate voltage:	6 kV

<u>Aperture Dimensions</u>

Stripping cell length:	26 cm
Snubber length:	6 cm
Cell-to-snubber exits distance:	30 cm
Snubber to anode #1 distance:	6.8 cm
Mass column length:	40 cm
Pole-to-MCP drift distance:	15 cm
Stripping cell aperture:	4.64 mm (ΔE) x 1.5 mm (ΔM)
Snubber aperture:	6 mm diameter
Maximum ion trajectory:	162 cm (snubber exit to anode #75)

TABLE II

MICROCHANNEL PLATE SPECIFICATIONS

Mechanical

Pore diameter	25 μ
Channel bias angle:	$8^o/8^o$
Chevron interspace:	0.002 inches
Anode interspace:	0.015 inches

Electrical

Gain:	1×10^7
Pulse height FWHM	120%
Dark count	1 cps/cm^2
Strip current	30 μA
Maximum linear anode current:	~ 0.015 μA/cm^2
Maximum pulse count rate:	10^6 cps (random per 0.4cm x 1.0 cm anode)

REFERENCES

1 N.C. Luhmann, Jr. and W.A. Peebles, “Instrumentation for Magnetically Confined Fusion Plasma Diagnostics,” Rev. Sci. Instrum. **55**, 279 (1984).

2 C.B. Wharton, “A Review of Energetic Neutral Particle Plasma Diagnostics,” Proc. 1st Course on Diagnostics and Data Acquisition Systems, Varenna, Italy (1975), p. 70.

3 V.V. Afrosimov, I.P. Gladkovskii, Yu. S. Gordeev, I.F. Kalinkevich, and N.V. Fedorenko, “Method of Investigation of the Flux of Atoms Emitted by a Plasma,” Sov. Phys.-Tech. Phys. **5**, 1378 (1961). Also V.V. Afrosimov and I.P. Glakkovskii, Sov. Phys.-Tech. Phys. **12**, 1135 (1967).

4 Equipe TFR, “Tokamak Plasma Diagnostics,” Nucl. Fusion **18**, 647 (1978).

5 R. Kaita, R.J. Goldston, D. Meyerhofer, and J. Eridon, “Design and Calibration of the Fast Ion Diagnostic Experiment Detector on the Poloidal Divertor Experiment,” Rev. Sci. Instrum. **52**, 1795 (1981).

6 G. Becker, Z. Phys. **231**, 6 (1970).

7 S.S. Medley and D.R.A. Webb, “Ion Temperature Measurements for the PROTO-CLEO Stellarator using a Multi-grid Electrostatic Energy Analyser,” J. Phys. D: Appl. Phys. **4**, 658 (1971).

8 V.V. Afrosimov, E.L. Berezovskii, .I.P. Gladkovskii, IA. I. Kislyakov, M.P. Petrov, and V.A. Sadovnikov, Sov. Phys.-Tech. Phys. **20**, 33 (1975).

9 S.S. Medley, K. Bol, S.L. Davis, H.P. Eubank, R.J. Goldston, L.R. Grisham, R.J. Hawryluk, J.C. Hosea, E.B. Meservey, G. Schilling, W. Stodiek, R. Stooksberry, and M. Ulrickson. “Charge Exchange Measurements During Neutral Beam Injection and ICRF Heating on PLT,” in Proceedings of the Ninth European Conference on Controlled Fusion and Plasma Physics (Culham Laboratory, Abingdon, Oxfordshire, UK, 1979) Vol. **I**, p. 48. Also, S.S. Medley and S.L.

Davis, “Charge Exchange Ion Temperature Measurements during High Power Neutral Beam Injection on PLT,” PPPL Report-1507, (1979) 41 pp.

10 D.E. Post, L.R. Grisham, and S.S. Medley, “A Technique for Measuring the Fast $^{3}He^{++}$ Distribution during $^{3}He^{++}$ Minority ICRF Heating,” Nucl. Technol./Fusion **3,** 457 (1983). Also, S.S. Medley, “Use of the Prototype TFTR Charge Exchange Analyzer for Fast $^{3}He^{++}$ Diagnostics During ICRF Heating on PLT,” PPPL-1770 (1981) 18 pp.

11 S.S. Medley and R. Persing, “Response of a Chevron Microchannel Plate to 2.5 and 14 MeV Neutrons,” Rev. Sci. Instrum. **52**, 1463 (1981).

12 J.L. Wiza, “Microchannel Plate Detectors,” Nucl. Instrum. Methods **162**, 587 (1979).

13 A.L. Roquemore, G. Gammel, G.W. Hammett, R. Kaita, and S.S. Medley, “Application of an E Parallel B Spectrometer to PLT Charge Exchange Diagnostics,” Rev. Sci. Instrum. **56,** 1120 (1985).

14 S.L. Davis, D. Mueller, and C.J. Keane, “Mass Resolving Charge-exchange System on the Poloidal Divertor Experiment,” Rev. Sci. Instrum. **54**, 315 (1983).

15 R.J. Colchin, A.L. Roquemore, and S.D. Scott, “Charge Exchange Stripping Cell Measurements Over a Wide Pressure Range,” Rev. Sci. Instrum. **59**, 1667 (1988).

16 M.R. Wade, R.J. Colchin, J.F. Lyon, R.N. Morris, C E. Thomas, and A.L. Roquemore, “ATF Neutral Particle Analysis System,” Rev. Sci. Instrum. **61**, 3202 (1990).

17 C. Kurz, C.L. Fiore, “Neutral Particle Diagnostics for Alcator C-MOD,” Rev. Sci. Instrum. **61**, 3119 (1990).

18 K. Hayashi, K. Hashimoto, H. Yamoto, H. Takeuchi, Y. Miura, T. Nishitani, M. Shiho, and H. Maeda, “Charge Exchange Neutral Particle Mass and Energy Analyzer for the JT-60 Tokamak,” Rev. Sci. Instrum. **56**, 359 (March, 1985).

19 J.H. Foote, G. W. Coutts, L.R. Pedrotti, L. Schlander, and B.E. Wood, "E||B End-Loss-Ion Analyzer for Tandem-Mirror Experiment-Upgrade," Rev. Sci. Instrum. **56**, 1117 (1985).

20 A. Cote, Y. Demers, X. Litaudon, C. Cote, R. Decoste, V. Fuchs, D. Michaud, M. St-Onge, G. Abel, D. Boyd, P. Brooker, E. Haddad, P. Jacquet, J-L. Lachambre, H. H. Mai, F. Martin, G.W. Pacher, B. Quirion, N. Richard, I. P. Shkarofsky, M.M. Shoucri, F. Skiff, W. Zuzak, "Lower Hybrid Current Drive Experiments on the TdeV Tokamak," Proceedings of the 22nd European Physical Society Conference on Controlled Fusion and Plasma Physics, Bournemouth 1995, Volume **19C**, page II-361.

21 T. Fall, B. Terreault, G. Abel, A. Boileau, C. Liu-Hinz, A. Cote, H. Y. Guo, W.W. Zuzak, "Novel Isotope Exchange Scenarios: Investigation of Particle Recycling in the TdeV Tokamak," Plasma Phys. Control. Fusion **36**, (1994) 1763.

22 R. Bartiromo, G. Bracco, M. Brusati, G. Grosso, S. Mantovani, B. Tilia, and V. Zanza, "Design and Calibration of the JET Neutral Particle Analyzer," Rev. Sci. Instrum. **58**, 788 (1987).

23 H. Takeuchi, T. Matsuda, Y. Miura, M. Makoto, H. Maeda, K. Hashimoto, and K. Hayashi, "Multi-Channel Mass-Separated Neutral Particle Energy Analyser for Simultaneous Measurements of Hydrogen and Deuterium Atoms Emitted From Tokamak Plasma," Japanese Journal of Applied Physics **22**, 1709 (1983).

24 A.B. Izvozchikov, A.V. Khudoleev, M.P. Petrov, S. Ya Petrov, S.S. Kozlovskij, S. Corti, and A. Gondhalekar, "Charge-Exchange Diagnostic of Fusion Alpha Particles and ICRF Driven Minority Ions in MeV Energy Range in JET Plasma," JET Joint Undertaking, Abingdon, Oxfordshire, England, Report JET-R(91) 12, (1991).

25 W.A. de Zeeuw, H.W. van der Ven, J.M M. de Wit, and A.J.H. Donne, "An Electrostatic Time-of-flight Analyzer for Sumultaneous Energy and Mass Determination of Neutral Partcles," Rev. Sci. Instrum. **62**, 110-117 (1991).

26 G. Bracco, S. Mantovani, A Moleti, B. Tilia, V. Zanza, and G. Betello, "Design and Calibration of a Time of Flight Neutral Particle Analyser with Noise Rejection Capability," EURATOM-ENEA Report ISSN/1120-5598 (1992) 52 pp.

27 A.L. Roquemore and S.S. Medley, "Design Concepts for Compact Mass/Energy Charge Exchange Analyzers," Rev. Sci. Instrum. **57**, 1797-1799 (1986).

28 C.J. Armentrout, "Design Study for a Compact E||B Particle Spectrometer," Rev. Sci. Instrum. **61**, 3098 (1990).

29 C.J. Armentrout, G. Bramson, and R. Evanko, "E Parallel B Canted Detector Neutral-Particle Spectrometer," Rev. Sci. Instrum. **56**, 2101 (November, 1985).

30 S.S. Medley, "Vacuum System Design and Tritium Inventory for the TFTR Charge Exchange Diagnostic," J. Vac. Sci. Technol. **A 4**, 97 (1986).

31 L.Lagin, S.S. Medley, and W. Bergin, "The TFTR Charge Exchange Diagnostic Software," IEEE Trans. Nucl. Sci. **NS-32**, 1268 (1985).

32 A.L. Roquemore and S.S. Medley, "Gyro-Electron Ghost Images Due to Microchannel Plate Operation in Transverse Magnetic Fields," Rev. Sci. Instrum. **57**, 2966 (1986).

33 A.L. Roquemore, S.S. Medley, and S.D. Scott, "Design and Performance Characteristics of the Radiation Shield Developed for the TFTR Charge Exchange Diagnostics," Rev. Sci. Instrum. **59,** 1726 (1988).

34 M.E. Malinowski, "The Response of a Microchannel Plate to Low Pressure Gaseous Tritium," Sandia Report SAND82-8831 (1992) 37 pp.

35 S.S. Medley, "Performance Study of Diagnostic Neutral Beam for Active Charge Exchange Measurements on the Tokamak Fusion Test Reactor," Fusion Technol. **11**, 346 (1987).

36 C.F. Barnett, J.A. Ray, E. Ricci, M.I. Wilker, E.W. McDaniel, E.W. Thomas, and H. B. Gilbody, “Atomic Data for Controlled Fusion Research,” Oak Ridge National Laboratory Report ORNL-5206 (1977).

37 K.M. Young, M.G. Bell, W.R. Blanchard, N.L. Bretz, J.L. Cecchi, J. Coonrod, S.L. Davis, H.F. Dylla, P.C. Efthimion, R.J. Fonck, R.J. Goldston, D.J. Grove, R.J. Hawryluk, H.W. Hendel, K.W. Hill, J. Isaacson, L.C. Johnson, R. Kaita, R.B. Krawchuk, R. Little, M.P. McCarthy, D.C. McCune, K. McGuire, D.M. Meade, S.S. Medley, D. Mikkelsen, D. Mueller, E. Nieschmidt, D.K. Owens, A.T. Ramsey, A. L. Roquemore, L.E. Samuelson, N.R. Sauthoff, J. Schivell, J.A. Schmidt, S. Sesnic, J. Sinnis, J.D. Strachan, G.D. Tait, G. Taylor, F.H. Tenney, and M. Ulrickson, “TFTR Initial Operations,” Plasma Phys./Control. Fusion **26**, 11 (1984).

38 S.S. Medley, M. Bitter, A.C. England, E. Fredrickson, S. von Goeler, R.J. Goldston, G.W. Hammett, R.J. Hawryluk, H.W. Hendel, K.W. Hill, R. Kaita, S.M. Kaye, K. McGuire, D.M. Meade, M. Murakami, E.B. Nieschmidt, A.L. Roquemore, S.D. Scott, J.D. Strachan, G.D. Tait, C.E. Thomas, K.L. Wong, K.M. Young, and M.C. Zarnstorff, “Ion Behavior in TFTR During Ohmic and Neutral Beam Operation,” in Proceedings of the Twelfth European Conference on Controlled Fusion and Plasma Physics, (Budapest, Hungary, September 1985) (European Physical Society, Budapest, Hungary, 1985) edited by L. Pocs and A. Montral, Part I, p. 343.

39 R. Kaita, W.W. Heidbrink, G.W. Hammett, A.A. Chen, A.C. England, H.W. Hendel, S.S. Medley, E. Nieschmidt, A.L. Roquemore, S.D. Scott, J.D. Strachan, G.D. Tait, G. Taylor, C.E. Thomas, and K.L. Wong, “Charge-Exchange and Fusion Reaction Measurements During Compression Experiments With Neutral Beam Heating in the Tokamak Fusion Test Reactor,” Nucl. Fusion **26**, 863 (1986).

40 G.W. Hammett, R. Kaita, J.R. Wilson, “Measurements of Energetic Helium-3 Minority Distributions during Ion Cyclotron Radio frequency Heating in the Princeton Large Torus,” Nucl. Fusion, **28**, 2027 (1998).

41 G.W. Hammett, W. Dorland, R. Kaita, S.S. Medley, D.N. Smithe, and P.L. Colestock, “Analysis of Charge Exchange Measurements During ICRF and ICRF+NBI Heating in TFTR,” in Proceedings of the Eighth Topical Conference on Applications of Radio-Frequency Power in Plasmas, (Irvine, CA, May 1989) American Institute of Physics **190**, 258 (New York, NY, 1989).

42 R. Kaita, G.W. Hammett, G. Gammel, R.J. Goldston, S.S. Medley, S.D. Scott, and K.M. Young, “Measurements with Vertically Viewing Charge Exchange Analyzers During Ion Cyclotron Range of Frequencies Heating in TFTR,” Rev. Sci. Instrum. **59,** 1691 (1988).

43 R. Kaita, R.B. White, A.W. Morris, E.D. Fredrickson, K. McGuire, S.S. Medley, and S D. Scott, “Mode Particle Resonances during Near-Tangential Neutral Beam Injection in the Tokamak Fusion Test Reactor,” Phys. Fluids B, **2**, 1584 (1990).

44 R.H. Radeztsky, S.D. Scott, R. Kaita, R.J. Goldston, G.W. Hammett, E. Fredrickson, S.S. Medley, R.J. Fonck, K.W. Hill, A.T. Ramsey, A.L. Roquemore, and M.C. Zarnstorff, “Measurements of Fast Ion Radial Diffusion in TFTR,” in Proceedings of the Fifteenth European Conference on Controlled Fusion and Plasma Heating, (Dubrovnik, Yugoslavia, May 1988) Vol. **12B**, Part 1, pp. 79-82.

45 W.W. Heidbrink, C.W. Barnes, G.W. Hammett, Y. Kusama, S.D. Scott, M.C. Zarnstorff, L.C. Johnson, D. McCune, S.S. Medley, H.K. Park, A.L. Roquemore, J.D. Strachan, and G. Taylor, “The diffusion of Fast Ions in Ohmic TFTR Discharges,” Phys. Fluids **B3**, 3167 (1991).

46 Y. Kusama, W.W. Heidbrink, C.W. Barnes, M. Beer, G.W. Hammett, D.C. McCune, S.S. Medley, S.D. Scott, and M.C. Zarnstorff, “Fast-Ion Radial Diffusivity Evaluated from Vertical Neutral Particle Measurements Following Short Pulse Beam Injection into a TFTR Ohmic Plasma,” PPPL Report-2813 (1992) 16 pp.

47 H.W. Kugel, H.P. Eubank, G. Gammel, L.R. Grisham, R. Kaita, J.H. Kamperschroer, T.A. Kozub, R. Langley, S.S. Medley, T. O'Connor, B. Prichard, Jr., A.L. Roquemore, and M.D. Williams, “Diagnostics for TFTR Neutral Beam Species Measurements,” Rev. Sci. Instrum. **57**, 2066 (1986).

48 H.W. Kugel, G.M. Gammel, L.R. Grisham, R. Kaita, J.H. Kamperschroer, R.A. Langley, C.W. Magee, S.S. Medley, T. Murphy, A.L. Roquemore, and M.D. Williams, “Measurements of Neutral Beam Species, Impurities, Spatial Divergence, Energy Dispersion, Pressure, and Reionization Using the TFTR U.S. Common Long Pulse Ion Source,” Rev. Sci. Instrum**.** **60**, 37 (1989).

49 C.L. Fiore, S.S. Medley, G.W. Hammett, R. Kaita, A L. Roquemore, and S. Scott, “Ion Temperature From Tangential Charge Exchange Neutral Analysis on the Tokamak Fusion Test Reactor,” Nucl. Fusion **28**, 1315 (1988).

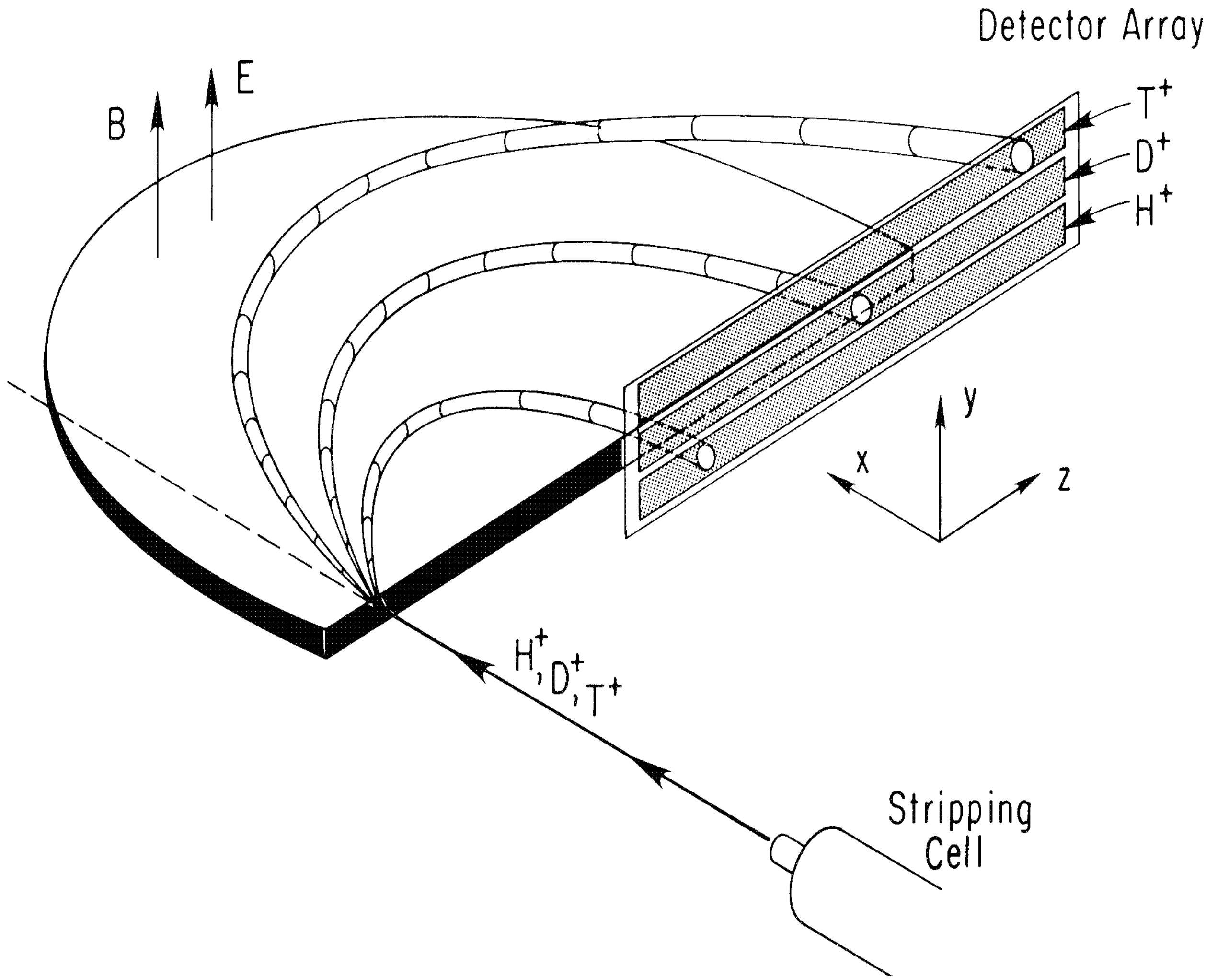

Fig. 1 Illustration of the superimposed electric and magnetic field E||B spectrometer concept.

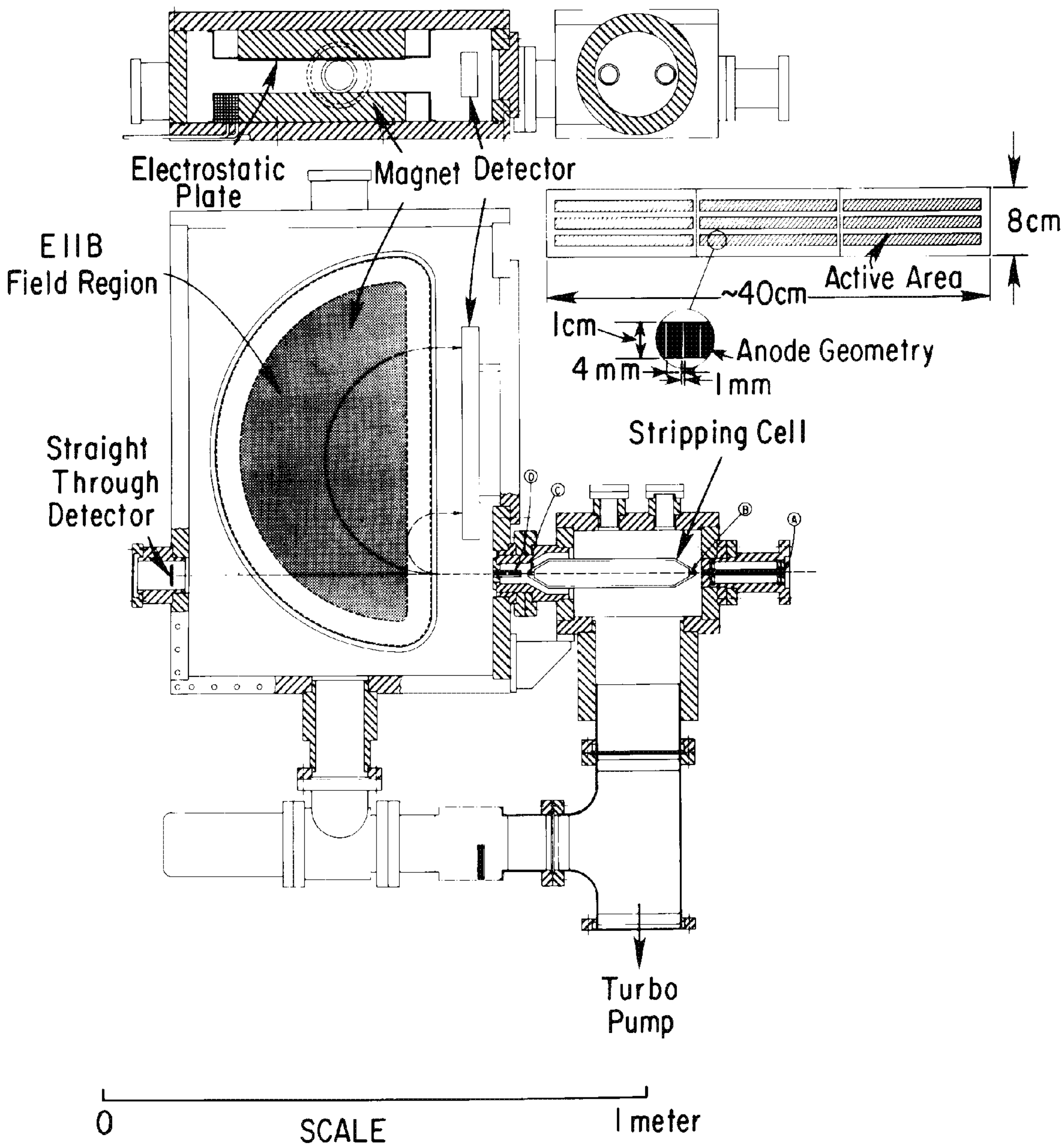

Fig. 2 Schematic of the EIIB spectrometer design.

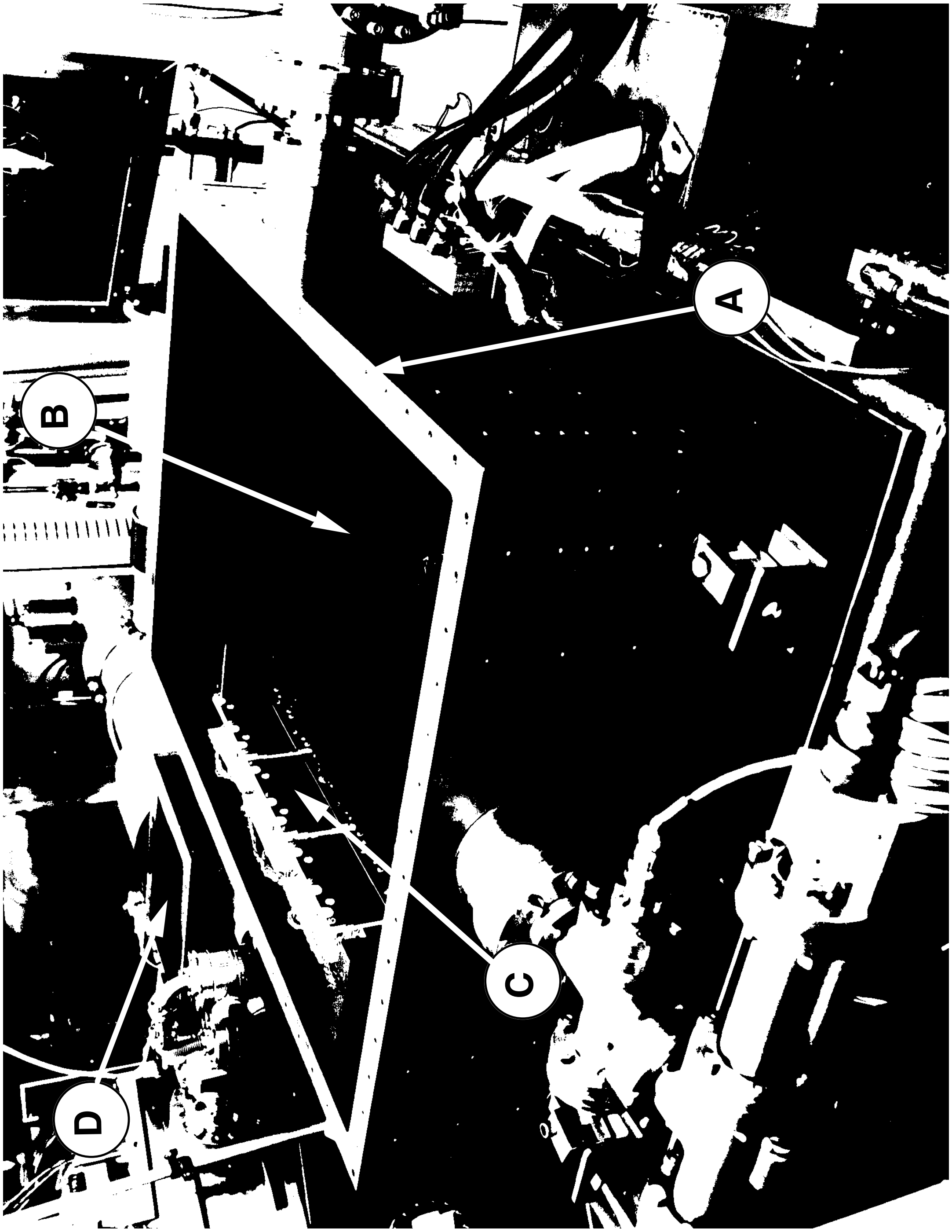

Fig. 3 Photograph of the E||B spectrometer with the magnet pole piece on one side removed to provide a view of the interior. Some of the major components labeled are: A) soft-iron walled spectrometer vacuum chamber, B) dee-shaped magnet pole, C) microchannel plate detector array, and C) stripping cell chamber.

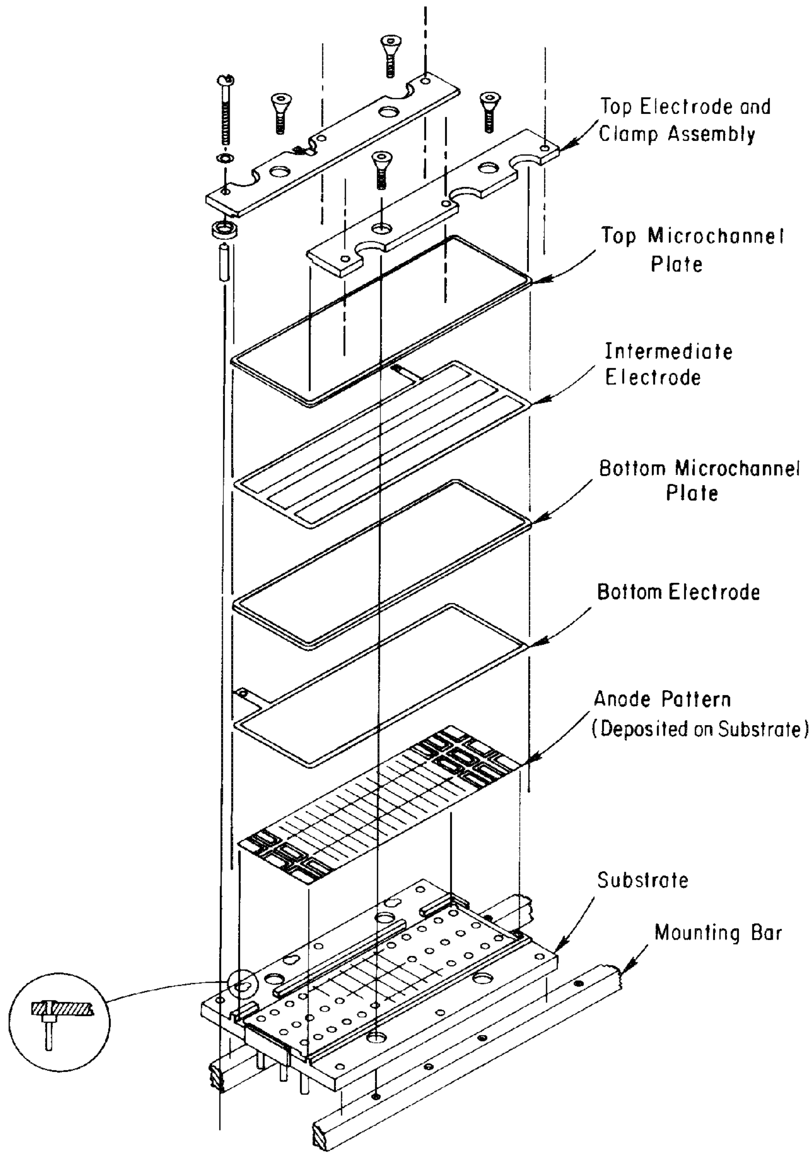

Fig. 4 Isometric assembly drawing illustrating the components of the multianode chevron channel electron multiplier array (CEMA) detector. Electrical contact with the anode pads is by means of pins extending through the backside of the ceramic substrate.

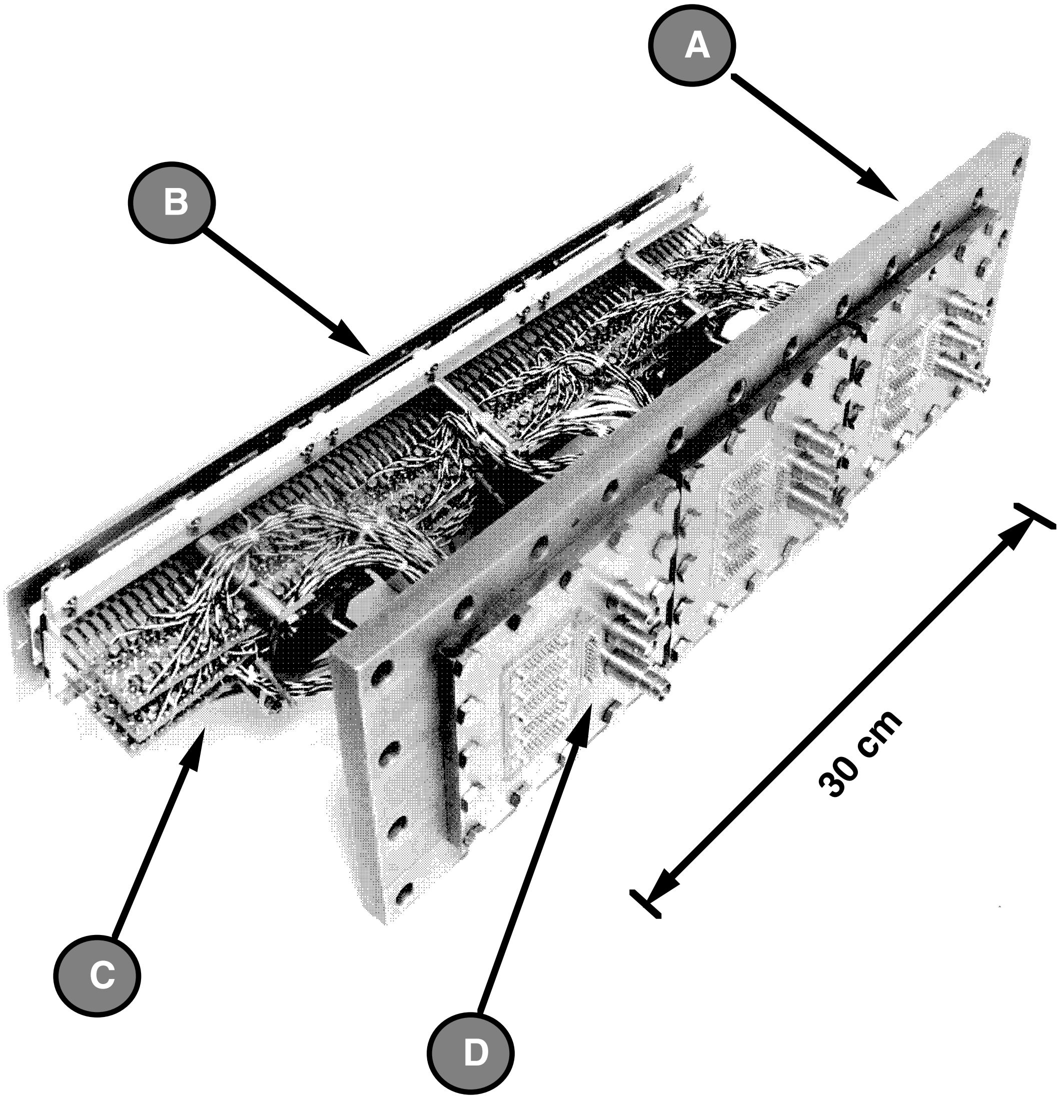

Fig. 5 Photograph of the microchannel plate and in-vacuo electronics module. Some of the major components labeled are: A) module assembly vacuum flange, B) microchannel plate (MC) detectors, C) in vacuo charge-to-voltage convertors, and D) feedthroughs for the MCP plate bias voltages (SHV connectors) and signal output (multi pin connectors).

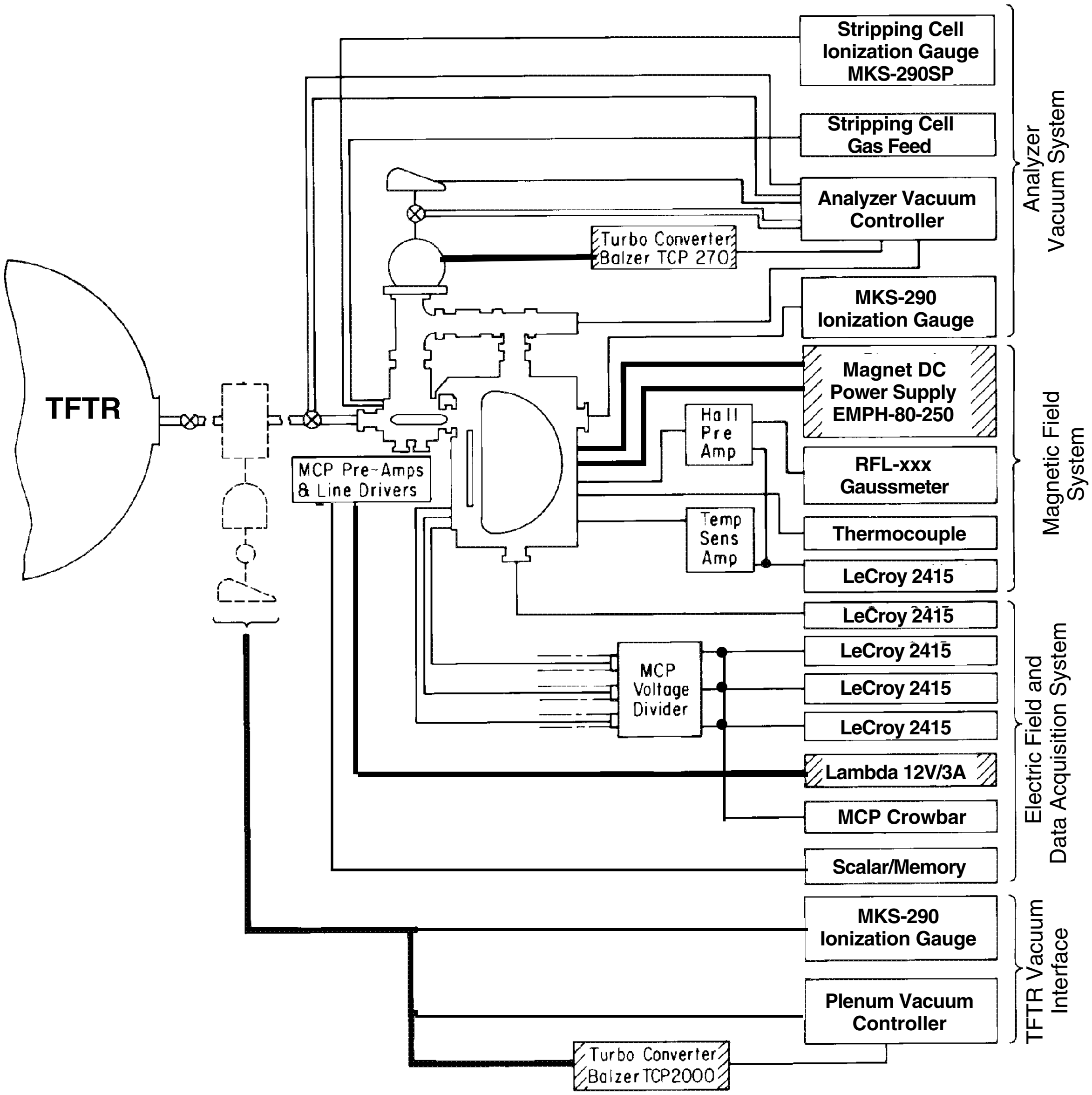

Fig. 6 Electronic and instrumentation block diagram for an E||B spectrometer installed on TFTR.

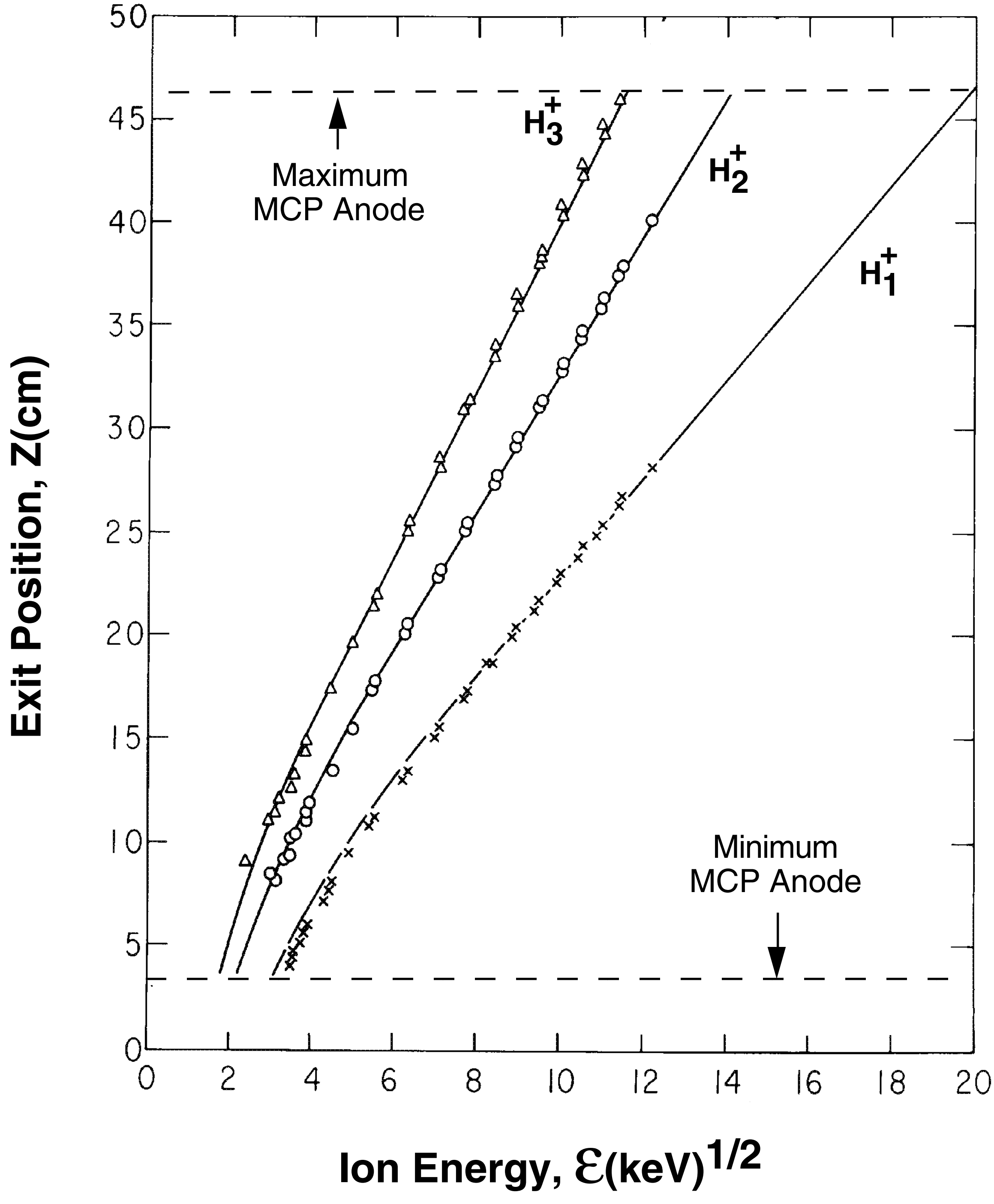

Fig. 7 Calibration results for the E||B analyzer showing the location of the ion beam on the detector plane as a function of ion energy (B = 2.7 kG, V = 1.1 kV).

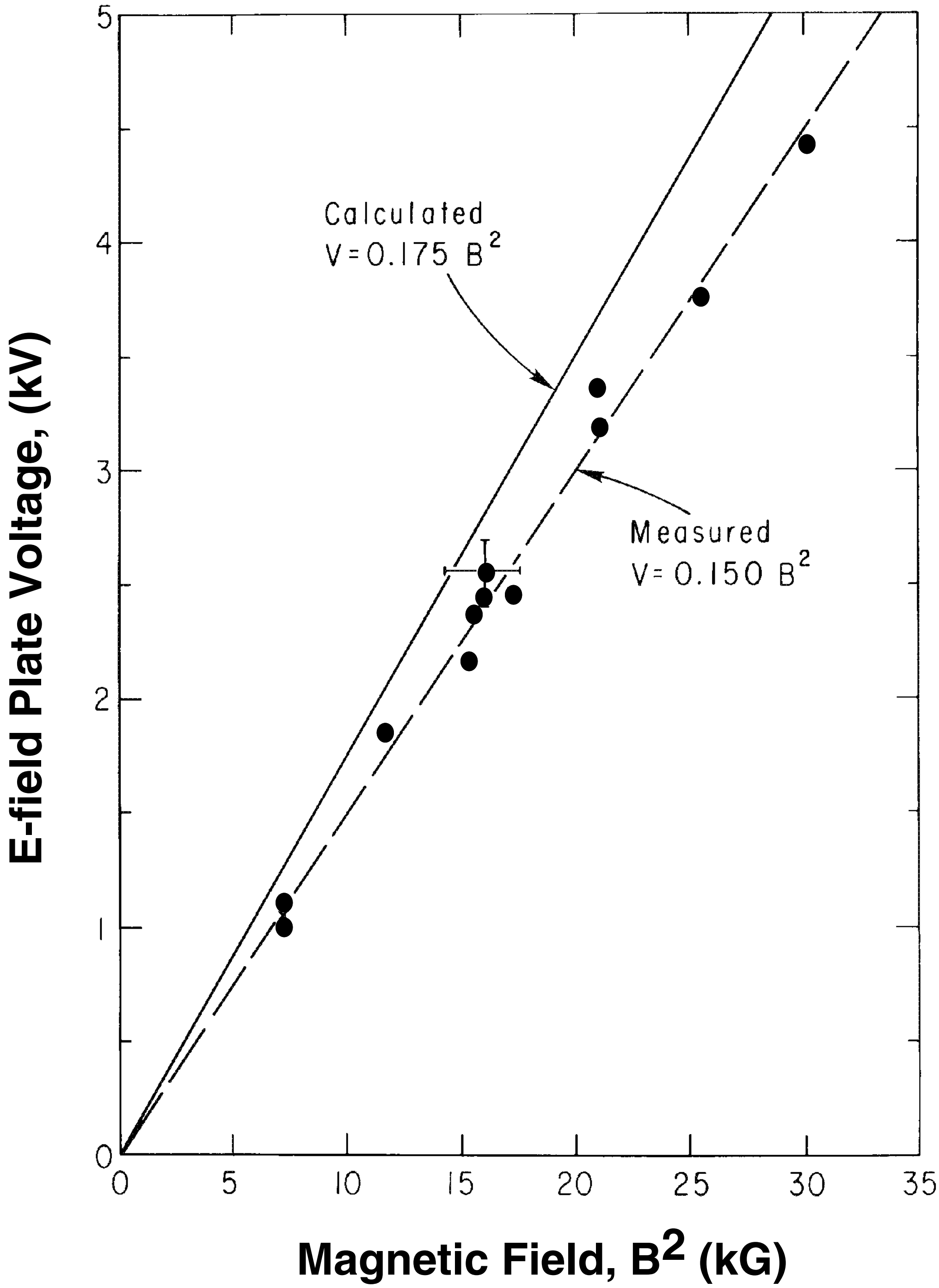

Fig. 8 Relationship between the operational values of the electric and magnetic fields for the E||B spectrometer.

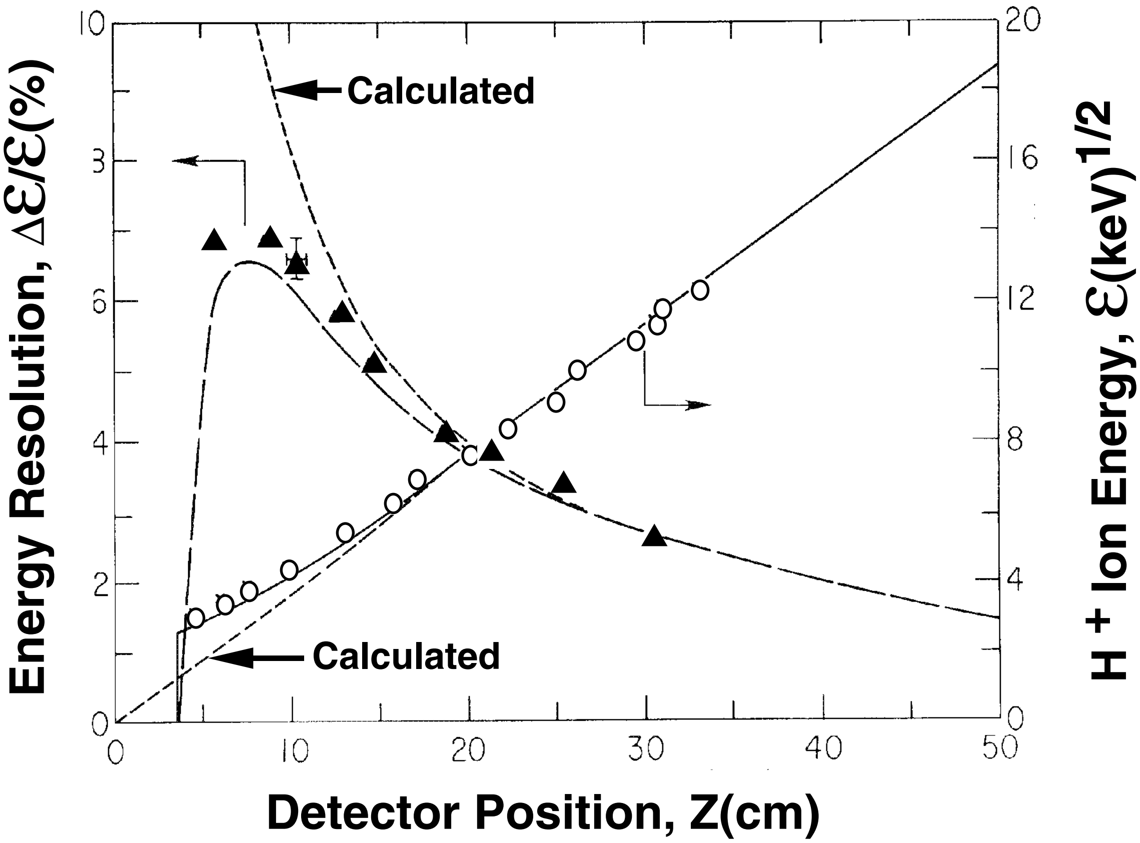

Fig. 9 H^+ calibration results for the E||B analyzer showing the energy resolution (left) and ion energy (right) as a function of position in the detector plane (B = 3.4 kG, V = 1.7 kV). The deviation from calculated behavior at low end of the detector is due to the "flyback effect" in the exit magnetic fringe field.

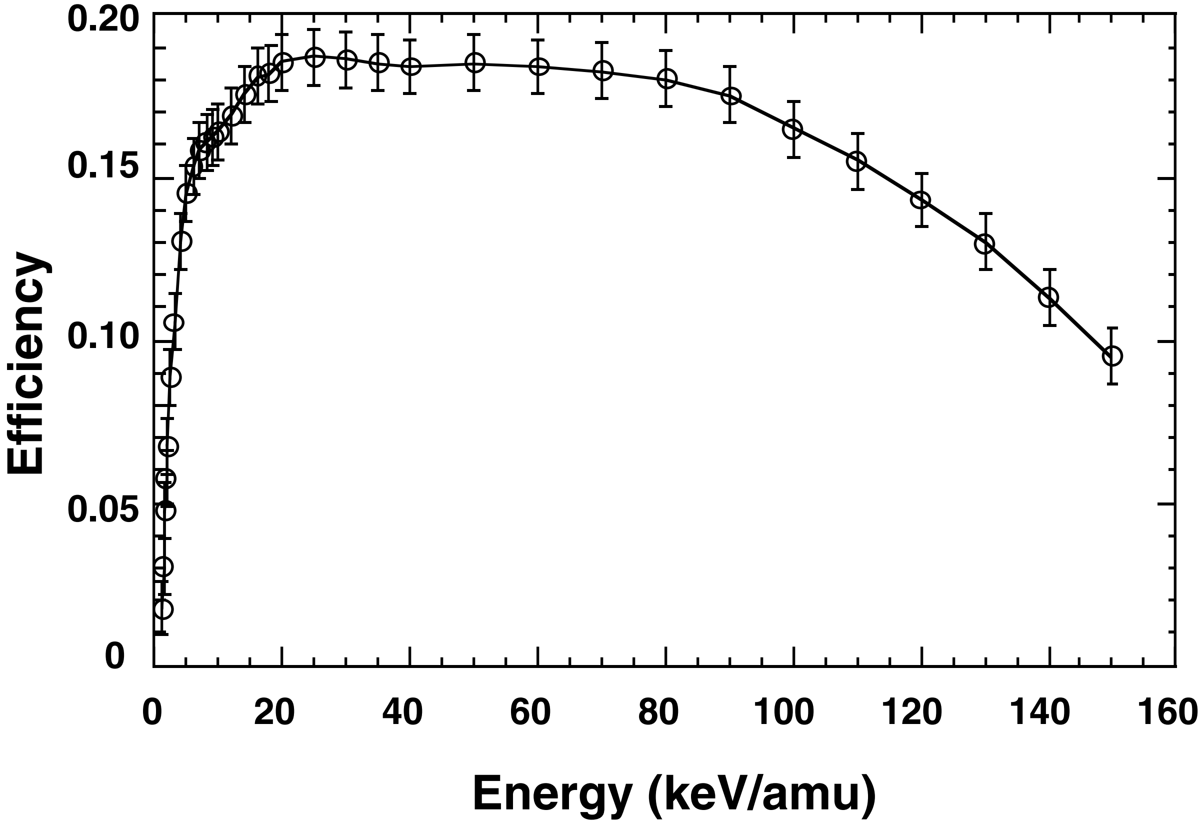

Fig. 10 Detection efficiency calibration data for the E||B spectrometer. The scatter in the data points reflects the variation arising from calibration of four separate spectrometer systems.

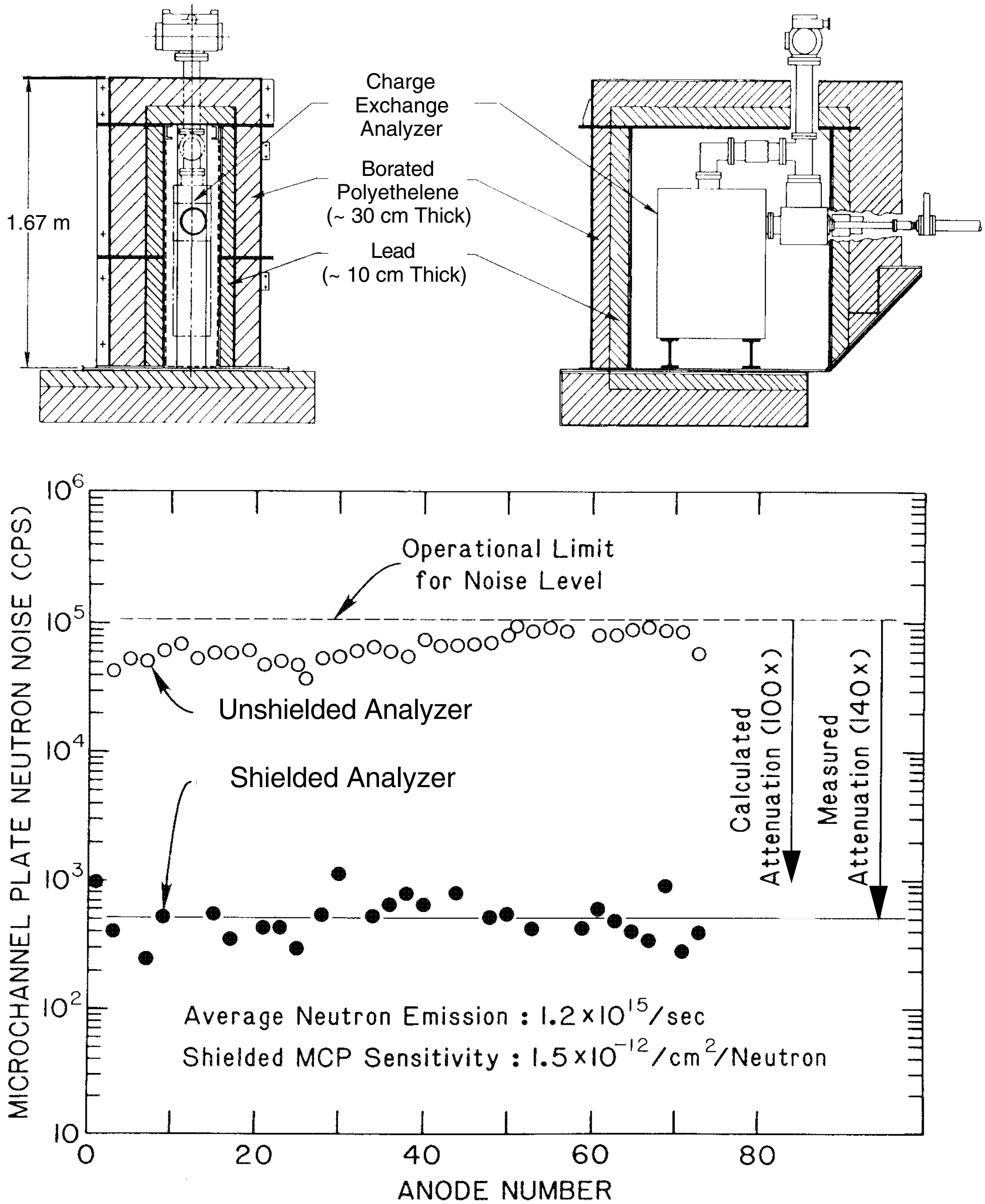

Fig.11 Schematic of the radiation shield for the TFTR EllB spectrometer (top) and comparison of the background neutron and gamma noise levels obtained for the shielded and unshielded analyzers (bottom).

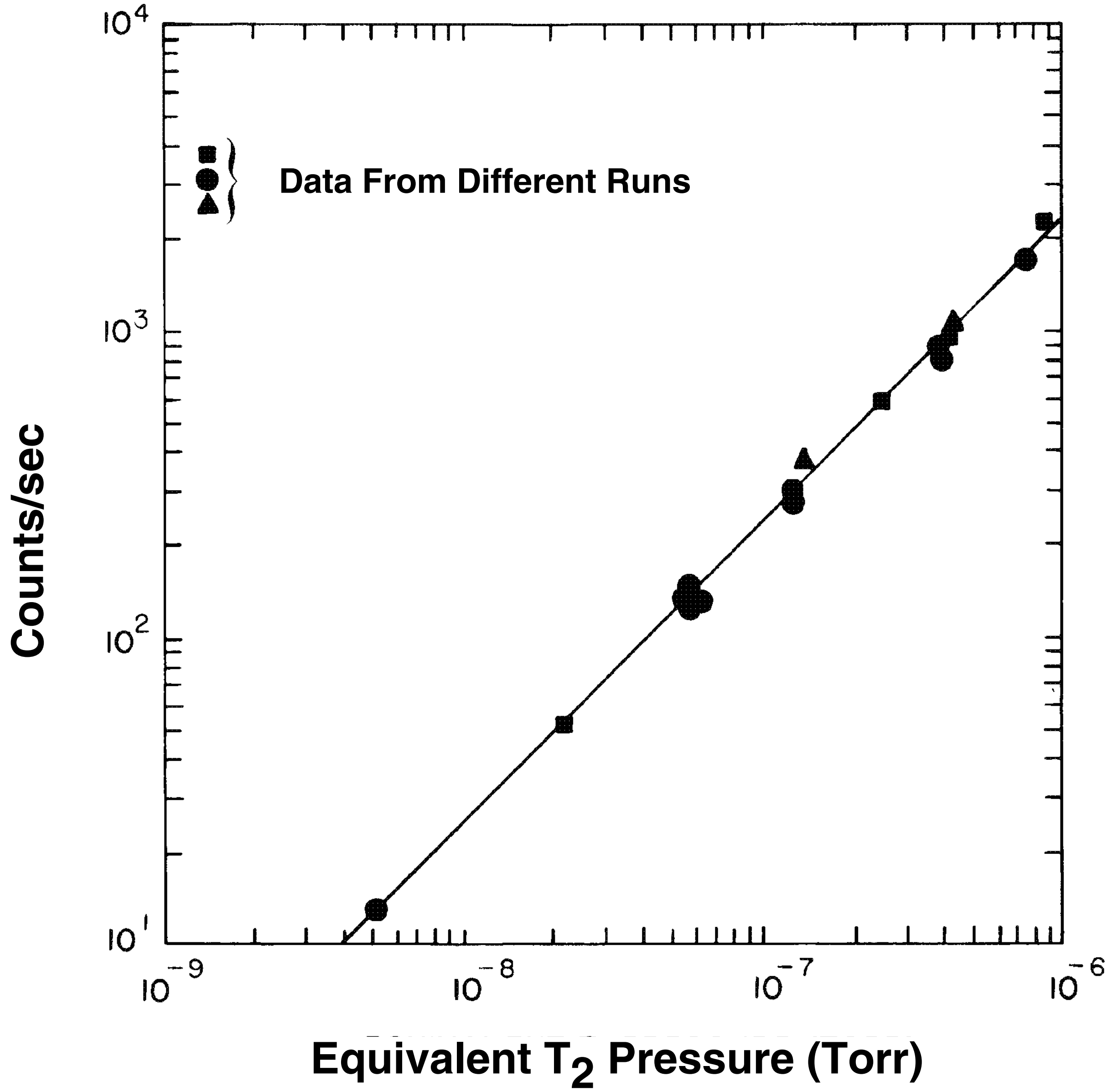

Fig. 12 The reversible tritium-induced microchannel plate counting rate as a function of tritium exposure pressure.

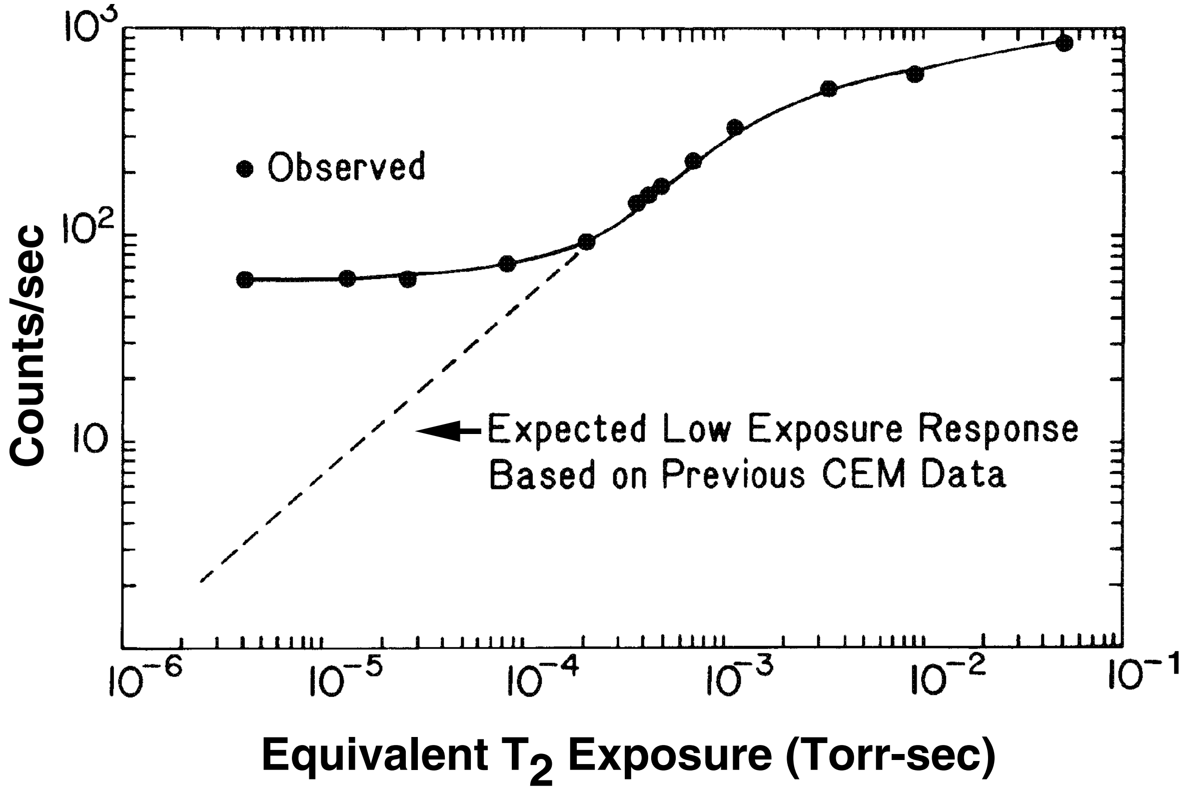

Fig. 13 The irreversible tritium-induced microchannel plate counting rate as a function of total tritium exposure.

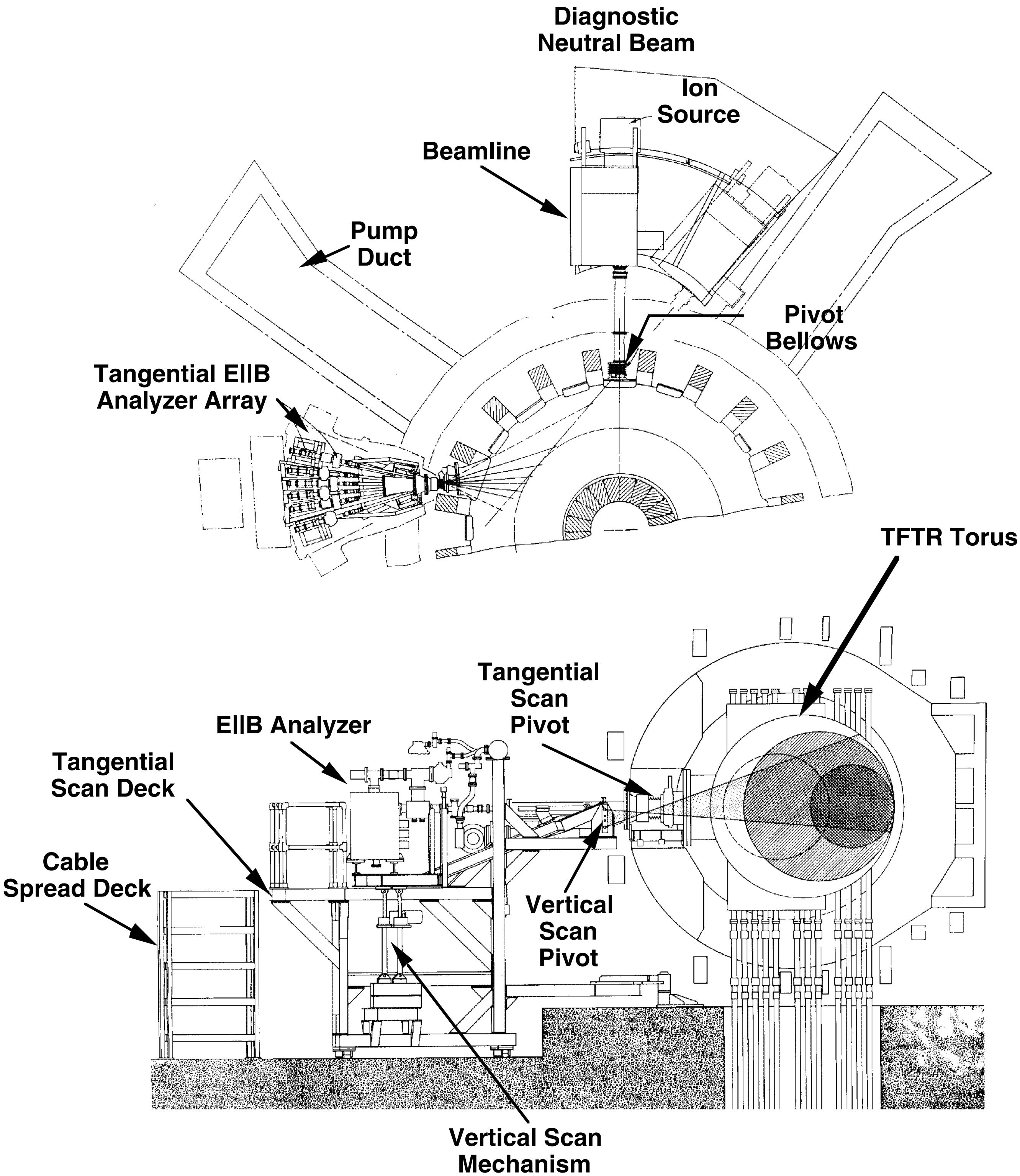

Fig. 14 Layout of the tangential charge exchange array on TFTR in plan (top) and elevation (bottom) views.

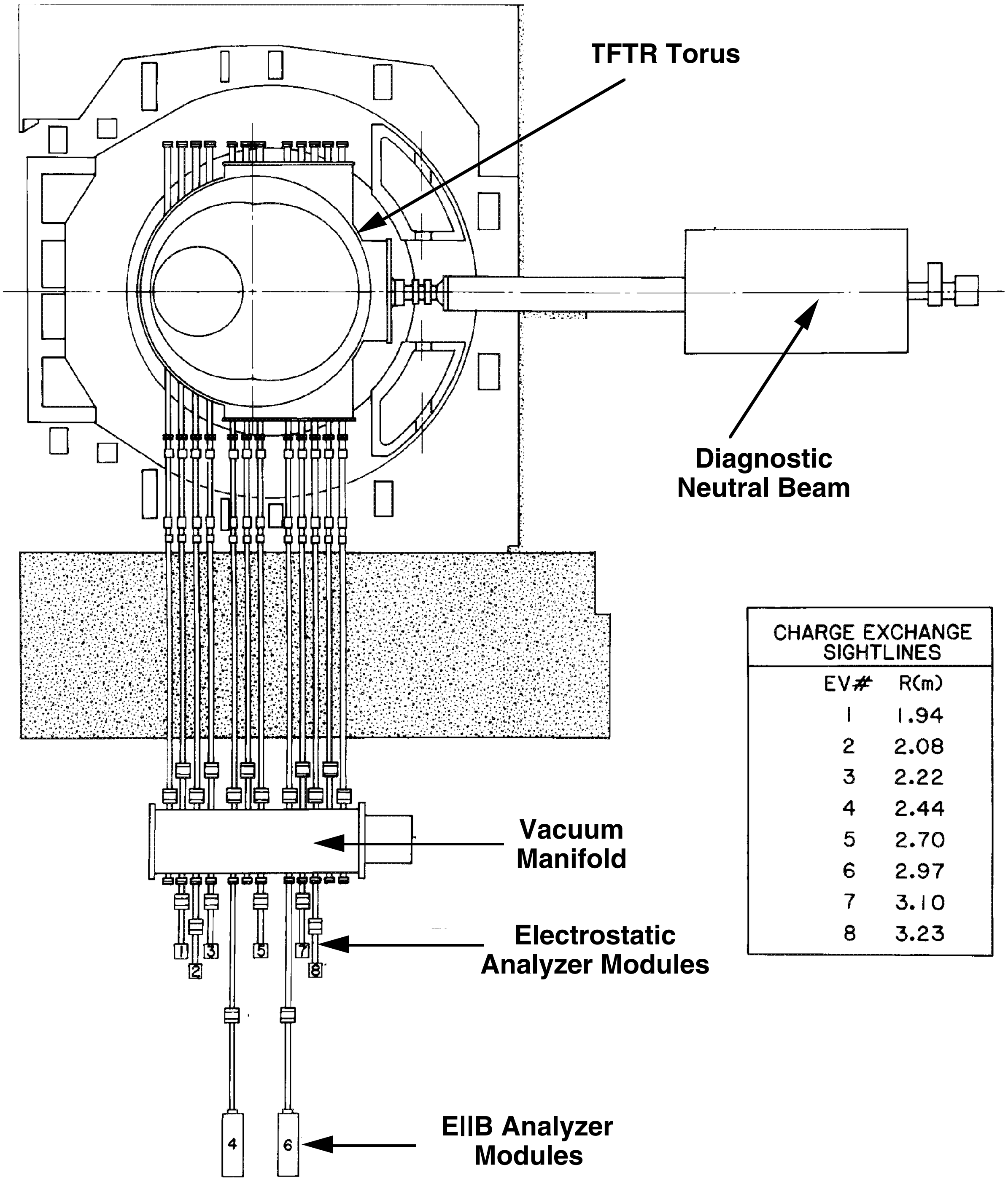

EV#	R(m)
1	1.94
2	2.08
3	2.22
4	2.44
5	2.70
6	2.97
7	3.10
8	3.23

Fig. 15 Elevation layout of the vertical charge exchange array on TFTR.

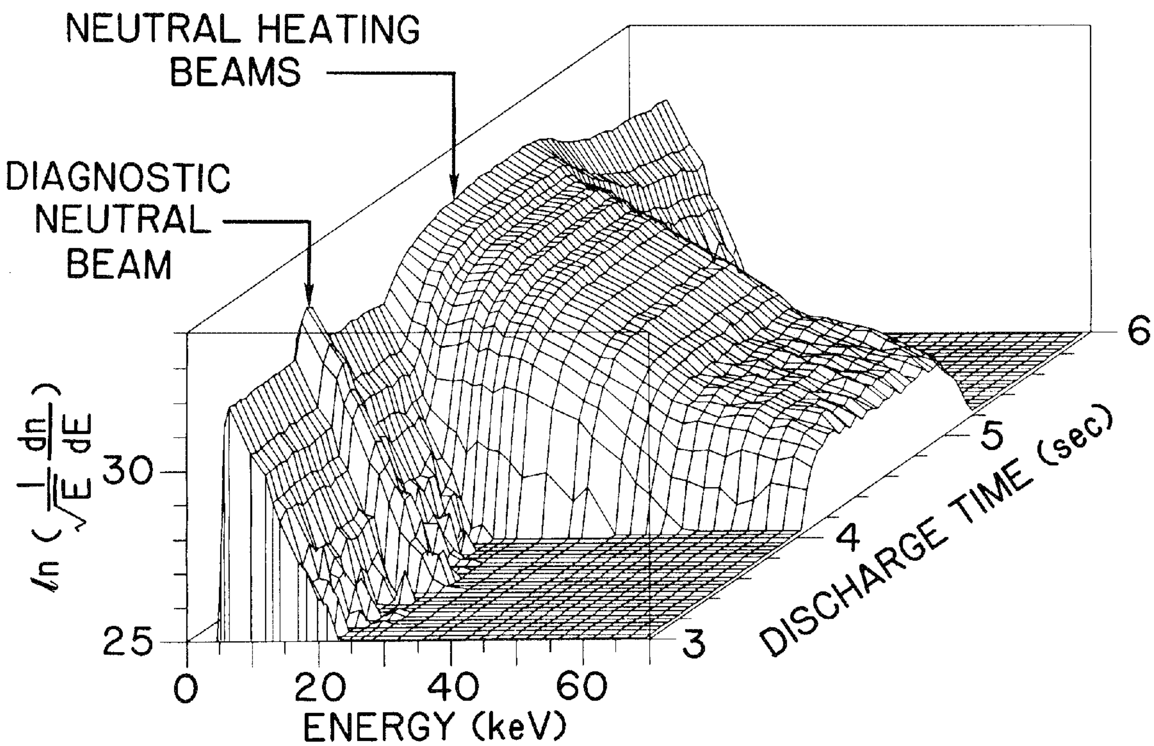

Fig. 16 E||B analyzer deuterium spectra in the energy range of 5 - 70 keV during deuterium neutral beam injection between 4.0 and 5.0 s into a deuterium plasma. Also shown is the active charge exchange signal enhancement produced by the diagnostic neutral beam during the ohmic phase preceding NBI heating.

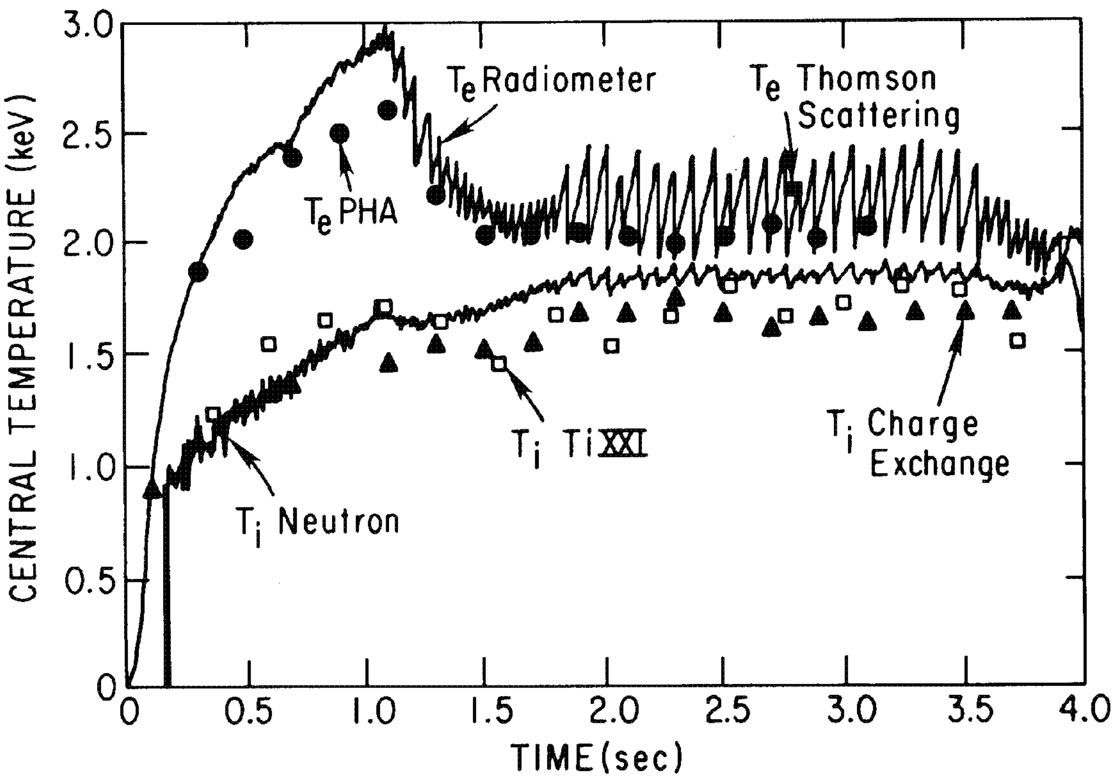

Fig. 17 Passive charge exchange measurements in an Ohmic discharge and comparison with X-ray crystal spectrometer and neutron results.

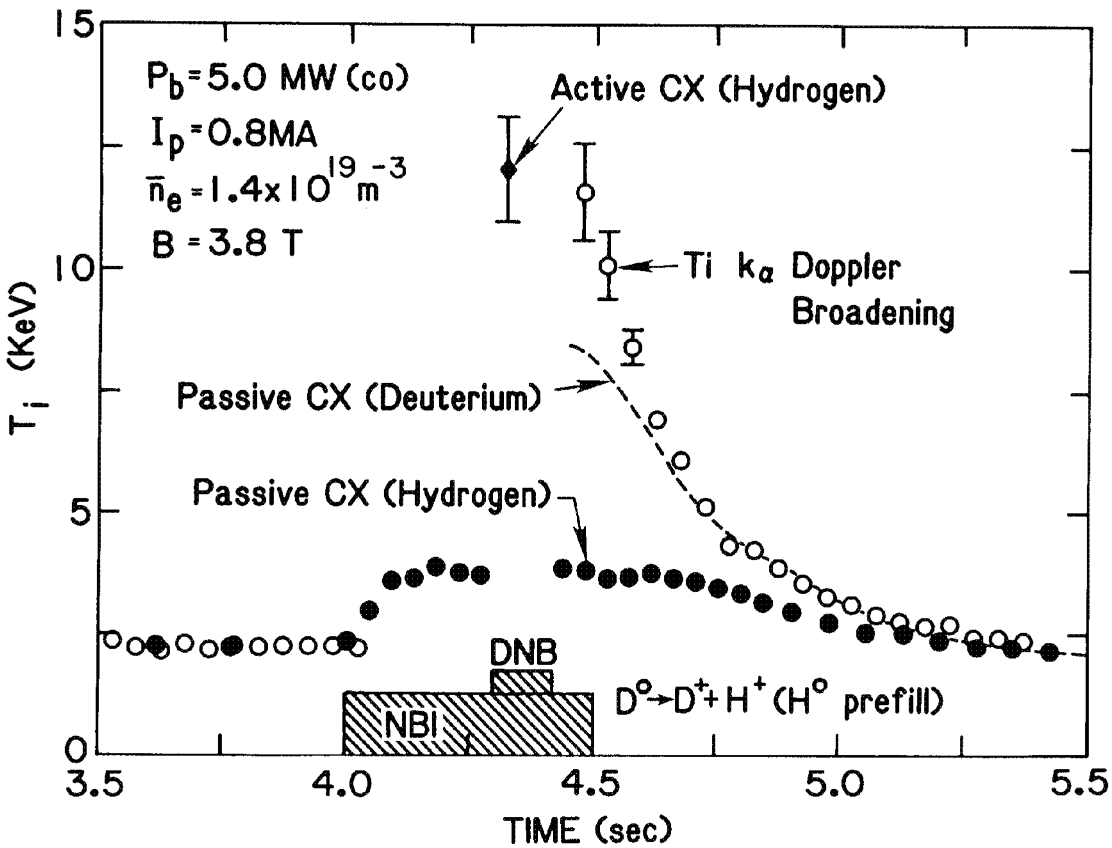

Fig. 18 Active charge exchange measurements obtained with the E||B spectrometer and comparison with results from the X-ray crystal spectrometer.

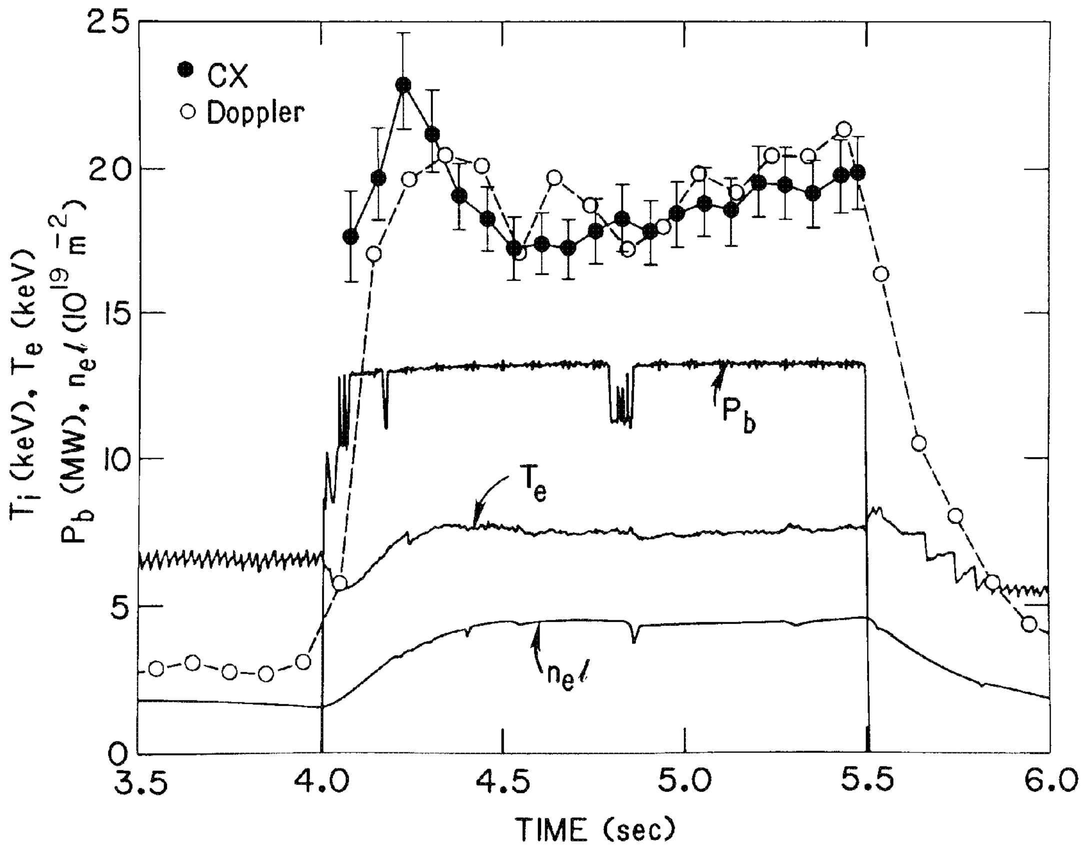

Fig. 19 Central ion temperature measured by the tangential supra-beam charge exchange technique (solid circles) in comparison with measurements from the horizontal X-ray crystal diagnostic using the Doppler broadening of the Ni XXVII K_α impurity line emission for a discharge with low toroidal rotation velocity ($v_\phi \leq 1.5 \times 10^5$ ms^{-1}). The toroidal rotation correction to the charge exchange data is small (< 7%) and has not been applied to the data.